Quantitative assessment of non-stationary relationship between multi-scale urban morphology and urban heat

Erdem Okumus, Deniz; Akay, Mert

DOI
10.1016/j.buildenv.2025.112669

Publication date
2025

Document Version
Final published version

Published in
Building and Environment

Citation (APA)
Erdem Okumus, D., & Akay, M. (2025). Quantitative assessment of non-stationary relationship between multi-scale urban morphology and urban heat. *Building and Environment*, *272*, Article 112669. https://doi.org/10.1016/j.buildenv.2025.112669

Building and Environment 272 (2025) 112669

Contents lists available at ScienceDirect

Building and Environment

journal homepage: www.elsevier.com/locate/buildenv

Quantitative assessment of non-stationary relationship between multi-scale urban morphology and urban heat

Deniz Erdem Okumus [a], Mert Akay [b,*]

[a] City and Regional Planning Department, Yildiz Technical University, Istanbul, Türkiye
[b] Department of Human-Centered Design, Delft University of Technology, Delft, the Netherlands

ARTICLE INFO

Keywords:
Urban morphology
Urban heat island
Heat heterogeneity
MGWR
Shap-explained xgboost
Istanbul

ABSTRACT

This study aims to quantify the impact of multiscale morphological features on urban heat heterogeneity by comparing linear (*Multiscale Geographically Weighted Regression -MGWR-*) and non-linear (*eXtreme Gradient Boosting -XGBoost-*) statistical models to decode global-local relationships and develop cooling strategies. The research followed a five-stage methodology: (1) hexagon-based sample selection, (2) urban heat extraction, (3) multiscale morphological measurements, (4) application of MGWR and SHAP-explained XGBoost, and (5) sensitivity analyses. Both models computed the model accuracy by employing three parameters, the coefficient of determination, the adjusted coefficient of determination, and the root mean square error, enabling the comparison of the linear-based and non-linear-based approaches. This framework addressed knowledge gaps related to model-specificity, statistical model performances, building granularity and urban network parameters impact, spatial heterogeneity in linear models, and interpretability challenges in machine learning outputs. XGBoost outperformed at modelling discrete spatial heterogeneity due to its tree-based algorithm, while MGWR effectively modelled continuous spatial heterogeneity. Both models consistently identified *ground area ratio* (GAR) and *number of plots* (UBP) as major contributors to urban heat. GAR and UBP showed a strong non-linear influence on urban heat. The non-linearity extracted by XGBoost initially showed an upward trend in temperatures, but a diminishing return at a higher value of GAR and UBP. Although building features showed a low individual impact, their negative correlation with urban heat suggested a cumulative cooling potential. The research underscores model-specific non-stationary relationships between urban morpho-space and localised urban heat, promoting a tailored examination of mitigation potentials over a 'one-size-fits-all' approach, guiding urban planners to optimise built-fabric for effective heat mitigation and improved urban thermal quality.

1. Introduction

Urban heat island (UHI) is the most evident thermal phenomenon characterised by elevated temperatures in urban areas compared to the rural surroundings or suburban areas, resulting from the modifications in land surface properties [1,2]. The compound impact of rising global temperatures and exacerbated UHI have become a critical threat to urban sustainability due to intensified extreme heat exposure [3]. An increasing number of cities globally have been experiencing this rising trend in urban heat and heat exposure. Therefore, advanced mechanisms to understand the driving factors of spatially morphological extent in the UHI formation have garnered significant attention from researchers [4,5] as a game changer in battling this new local/microclimate crisis [6]. Furthermore, decision-makers and administration authorities in metropolitan areas have initiated focusing on localising sustainable development goals (SDG), particularly *SDG11. climate action* and *SDG13. sustainable cities and communities*, by addressing the impact of urban morphology on excessive urban heat and promoting heat mitigation measures to improve the quality of urban life and urban sustainability [7].

Changes in heat storage capacity, airflow patterns, and thermal conductivity between surface and atmosphere – stemming from the spatial layout, architectural morphology, and building granularity – shape local/microclimates by increasing the positive radiation budget in urban areas and resulting in urban heat heterogeneity [8–11]. Comprehensive academic research has established a significant impact of common urban morphology on land surface temperatures (LST) [11–13]. The most common attributes in the literature are ground area

* Corresponding author at: Faculty of Industrial Design Engineering, TU Delft Landbergstraat 15, CE 2628 Delft, the Netherlands.
E-mail address: m.a.akay@tudelft.nl (M. Akay).

https://doi.org/10.1016/j.buildenv.2025.112669
Received 26 October 2024; Received in revised form 21 January 2025; Accepted 3 February 2025
Available online 4 February 2025

ratio as a proxy of the building density in the 2D-morphology [2,14–16], and building height, building volume, sky view factor, floor area ratio, canyon geometry factor as proxies of the 3D-morphology [5,8,11,13,14,17–19]. Several variables regarding green vegetation intensity have also been included in the studies among the attributes of 2D-morphology [8,17,20]. Nevertheless, there is a knowledge gap for strong evidence about the relationship between urban heat, compositional level of building granularity and urban network enclosures, a black box to explore and clarify in the urban morpho-space. This gap constraints effective heat mitigation strategies for promoting climate-sensitive, -adaptive, and sustainable cities. Therefore, this research focuses on the multi-scale nature of urban morphology as a holistic urban morpho-space by adopting research variables belonging to plot layout and urban block morphology, building granularity and urban network at multi-planar levels.

Quantifying the relationship between multi-scale urban morphology and urban heat is challenging due to the complex interactions between the diverse textures, sizes, shapes and networks in the built environment, as well as the varying densities and arrangements of buildings across micro, local, and neighbourhood scales [7]. Literature underlines the case-specificity—often referred to as spatial non-stationarity—in quantitative research, which records inconsistent effects of morphological attributes regarding the impact magnitude and correlation direction (the sign of the coefficient) depending on specific spatial contexts [14,21,22]. Conventional statistical models generally presume spatial stationarity, generating variable estimates based on the assumption that relationships remain constant across space [23]. However, varying performances of adopted models – mostly conventional regression techniques – indicate uncertainties referring to the model-specificity or spatial non-stationary issues.

Relevant studies are widely conducted based on an assumption of linear relations, such as multiple linear regression models [14,24]. Even though such conventional approaches effectively model relationships between variables, they are limited to sensitivity to outliers, and multicollinearity and also overlook spatial heterogeneity, and spatial autocorrelation [5,25]. Geospatially adjacent areas often exhibit a certain level of similarity, whereas, in distinct regions, they demonstrate spatial variability [26]. Among the spatial statistical models, multi-scale geographically weighted regression (MGWR) captures spatial heterogeneity offering a more comprehensive explanation of the index coefficient's influence, and enhances the model's prediction capability [8,26–28].

Nonetheless, owing to the complexity of morphological attributes, linear models are pressingly insufficient to explain non-linear relationships between urban heat and morpho-metrics. Even though advanced statistical models, grounded in supervised machine learning (ML) algorithms, such as ridge regression, forest-based regressions, and regression trees, have been adapted to the UHI studies to enhance the predictive performance [11,12,15,29–32], only a few have highlighted such non-linear relationships [21,33–35]. eXtreme Gradient Boosting (XGBoost), a decision tree-based ensemble learning approach, is a novel framework to analyse complex non-linear relations and has a significant potential to explore the impact of morphological space on urban heat heterogeneity. The model's overall accuracy is enhanced by the objective function, which includes the loss function and regularisation terms; the loss function measures prediction errors, while regularisation mitigates overfitting (model bias) by controlling model complexity [17,36]. The model can rank the importance of features, quantify their impact and allow a deeper understanding of the contributions of various independent variables [17,37]. Ma et al. (2024) and Yuan et al. (2024) are single studies that performed XGBoost in the UHI context to analyse the influence of urban features on LST with an assumption of non-linear inter-relations. They, however, did not discuss the linear/non-linear dichotomy of morphological variables and presented certain limitations regarding the resolution of the indicators and scale dependency of the morphological metrics. There is a need for further discussion on the varying performances of the linear and the non-linear relationship between morpho-space metrics and urban heat heterogeneity which is another critical knowledge gap that this paper concentrates on.

The last critical knowledge gap in the literature is the challenge of interpretability in ML compared to spatial statistical models. According to Li (2022), ML is a black box in which the process and the results are particularly complex to comprehend. This challenge in geographical research leads researchers to conduct more interpretable spatial statistical models, even though there are other challenges on model-specificity, multicollinearity, spatial heterogeneity, spatial autocorrelation, and linear/non-linear dichotomy. Therefore, there is another need to adopt innovative techniques into ML workflows to present improved interpretations of ML outputs, providing detailed insights and additional explanations for feature importance. The cutting-edge development, the SHapley Additive exPlanations (SHAP) method, effectively illustrates the interrelations between variables and their impacts [38]. The method has already been used in environmental-based research, such as air pollution, energy consumption and hydro-climatological processes [39,40]. The integration and application of the SHAP method into ML workflows for UHI-based research represents another novel contribution of this study.

In short, this study addresses the following gaps in UHI research: (1) lack of strong evidence on the relationship between urban heat heterogeneity, building granularity and urban network enclosures, (2) overlooking the impact of spatial heterogeneity in the linear statistical models, (3) model-specificity regarding the varying performances of conventional-linear and advanced-non-linear models, and (4) the challenge of interpretability in ML outputs. Therefore, the research aims to better quantify the impact of multi-scale morphological features on urban heat heterogeneity by encouraging comparative evaluations of linear and non-linear statistical models to decode global and local relationships and develop relevant solutions. It employs a spatial statistical model, MGWR, and a SHAP-explained ML model, XGBoost, to discuss the better-fit model for describing the complexity of urban landscapes and the cooling benefits of the relationship between urban morphology and heat heterogeneity. Results fill the critical knowledge gaps in urban climate literature and enlighten the urban planning and design recommendations to regulate the urban thermal environment.

2. Methods

The research was conducted in five main stages: (1) hexagon-based sample selection, (2) urban heat extraction, (3) multi-scale morphological measurements, (4) employment of the spatial statistic model, MGWR, and the SHAP-explained ML model, XGBoost, and (5) sensitivity analyses, SHAP scores for XGBoost and Monte Carlo Simulation for MGWR results (Fig. 1).

2.1. Case area and hexagon-based sampling design

Istanbul (41.0°N, 28.9°E) is a metropolitan city located northwest of the country on two continents: Asia and Europe. The Black Sea surrounds the city on the north and the Marmara Sea on the south, which creates a certain cooling impact on the coastal areas (Fig. A.1). According to the Köppen climate classification, the city is a part of the hot and dry summer zone (Csa) [41]. Long-term averages in Istanbul demonstrate that the mean temperature is 25.5 °C in July, which is the hottest, and the heat island formation is the most prominent time, annually [42]. The city has been suffering from exponentially increased urban heat [43–45]. Morphologically heterogenic spatial patterns are seen as the principal factors of thermal conditions in urbanised areas [5,16].

A Hexagon unit was employed for the sampling design structure of the research. Accordingly, the metropolitan area was divided into hexagons with a side of 150 ms which covers several urban blocks and enables multi-scale evaluations through the morphological variables at

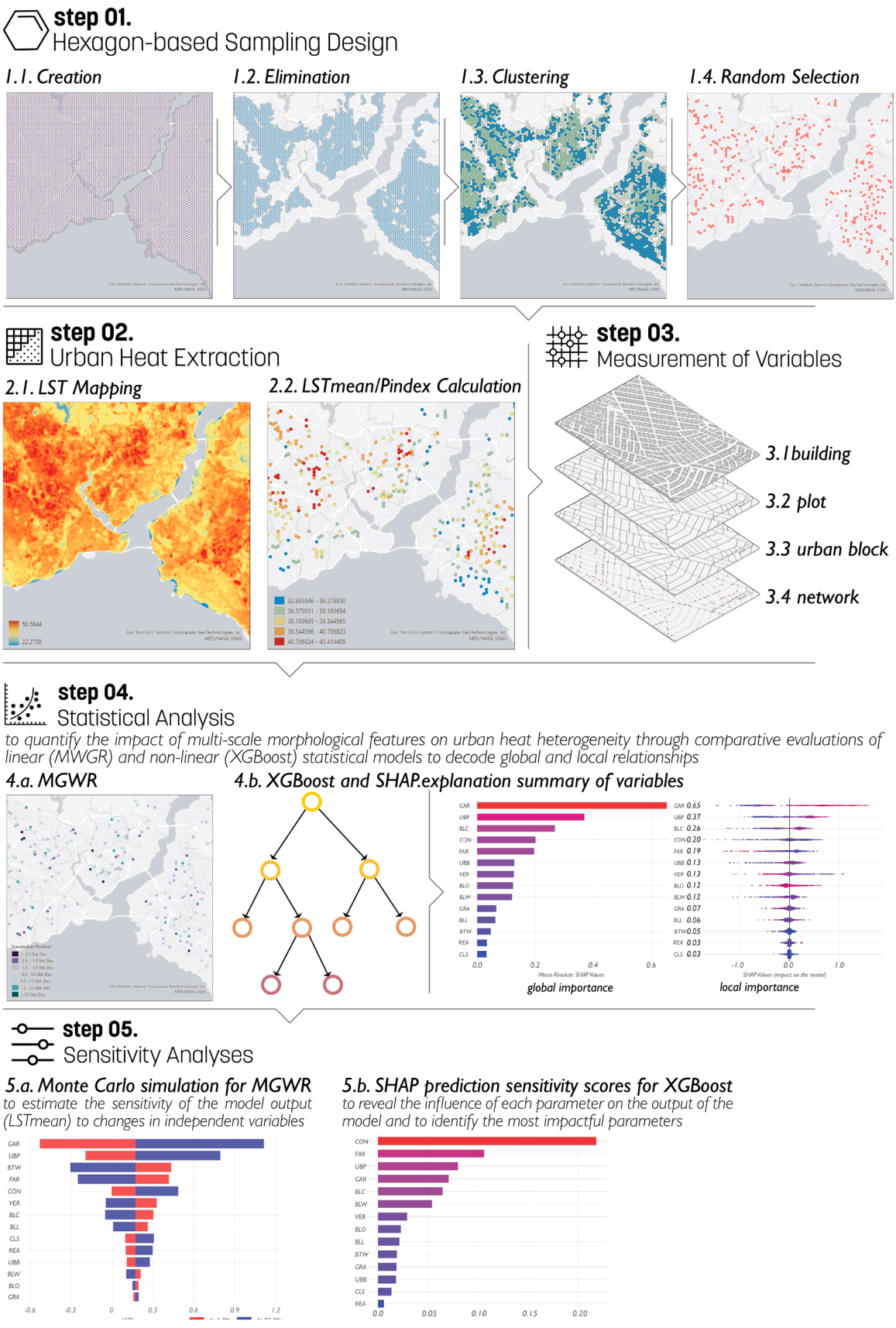

Fig. 1. Research design scheme.

the building, plot, and urban block scale. Although the square grids are the dominant spatial analysis unit in the current studies [46], the hexagons were employed for the research as they reduce sampling bias caused by edge effects of grid shapes [47,48]. Furthermore, administrative boundaries are subject to change over time, and spatial dynamics do not necessarily adhere to such rigid boundaries. Therefore, hexagons were selected over administrative boundaries due to their superior capacity to exhibit spatial variation.

Then, a pre-defined elimination procedure of 3-main-stages, exclusion-clustering-random selection, was applied to the hexagons through the following rules in an order:

(a) The exclusion stage consisted of the exclusion of the hexagon units outside the residential areas to eliminate the heterogeneity caused by land-cover variability, the exclusion of the hexagon units having hilly topography with an average slope over 25 % and the hexagon units located less than 1 km from a large water mass to eliminate the impact of natural drivers on hexagons [5].

(b) The clustering stage consisted of spatial clustering to identify natural clusters among the variables [49]. The analysis was conducted using the K-means algorithm [50], which does not require pre-classified features to detect clusters in the dataset. The K-Means algorithm is an unsupervised learning and clustering algorithm. Unsupervised learning is an ML technique whereby the model is not supervised; instead, it is required to work autonomously to discover information. In this context, the research used the GAR and FAR parameters, which indicate density in the second and third dimensions, to capture density-based spatial heterogeneity and represent morphological diversity in an urban landscape. Respectively, the following formulas were utilised during this analysis:

$$Pseudo\ F-statistic=\frac{\left(\frac{R^2}{n_c-1}\right)}{\left(\frac{1-R^2}{n-n_c}\right)} \tag{1}$$

where:

$$R^2=\frac{SST-SSE}{SST} \tag{2}$$

and SST reflects between-cluster differences and SSE reflects within-cluster similarity:

$$SST=\sum_{i=1}^{n_c}\sum_{j=1}^{n_t}\sum_{k=1}^{n_v}\left(V_{ij}^k-\overline{V^k}\right)^2 \tag{3}$$

$$SSE=\sum_{i=1}^{n_c}\sum_{j=1}^{n_t}\sum_{k=1}^{n_v}\left(V_{ij}^k-\overline{V_t^k}\right)^2 \tag{4}$$

where n represents the number of features, n_i shows the number of features in cluster i, n_j expresses the number of clusters, n_v indicates the number of variables used to cluster features. V_{ij}^k is the value of the k^{th} variable of the j^{th} feature in the i^{th} cluster, $\overline{V^k}$ denotes the mean value of the kth variable, and $\overline{V_t^k}$ exhibits the mean value of the k^{th} variable in cluster i.

Accordingly, three clusters are identified for the sample selection as follows:

- Cluster 1 - 3513 hexagon units: TAKS ranges 0.10–0.32, KAKS ranges 0.10–1.74
- Cluster 2 - 1297 hexagon units: TAKS ranges 0.13–0.72, KAKS ranges 1.25–9.26
- Cluster 3 −3016 hexagon units: TAKS ranges 0.11–0.54, KAKS ranges 0.38–3.23

(c) The random selection stage consisted of the sample size determination and random selection of feature subsets for each of the 3 clusters. The method of subset features is fundamentally an optimisation problem, implicating exploring the potential feature combinations to identify the optimal or near-optimal subset based on specific criteria [51–53]. According to the determined sample size with a confidence level of 95 % and a margin of error of 5 %, 343 hexagon units from Cluster 1, 297 hexagon units from Cluster 2, and 341 hexagon units from Cluster 3 were selected. Finally, 981 hexagon units in total were subjected to heat extraction, morphological measurements and statistical evaluations.

2.2. Urban heat extraction and p_{index} calculation

Urban heat heterogeneity was extracted from NASA's remotely sensed Landsat-8/9 multispectral data recorded on 26th July 2023 with 0 % land cloud coverage [54,55]. A series of algorithms to estimate the LST values were as follows [56–62]:

- Conversion to Top of Atmosphere (TOA) Radiance: Digital numbers (DN) of pixels in the thermal band (Band10 in Landsat-8/9) were converted to TOA spectral radiance by using rescaling factors (5).

$$L\lambda = MLQcal + AL \tag{5}$$

where L_λ is the TOA spectral radiance (watts/(m2*srad*μm)), M_L is the band-specific multiplicative rescaling factor, A_L is the band-specific additive rescaling factor, Q_{cal} is the quantised and calibrated standard product pixel values (DN). Owing to the calibration uncertainty of Band 11 (11.50 - 12.51 μm), solely Band 10 (10.60 - 11.19 μm) was utilised in this research [20,63].

- Conversion to Atmosphere Brightness Temperature (BT): The thermal band data were transformed from spectral radiance to top-of-atmosphere brightness temperature utilising the thermal constants (6).

$$T = K_2/(\ln((K_1/L_\lambda)+1) - 273.15 \tag{6}$$

where T is the TOA brightness temperature in kelvin (K), L_λ is the TOA spectral radiance, K_1 is the band-specific thermal conversion constant, K_2 is the band-specific thermal conversion constant.

- Normalised Difference Vegetation Index (NDVI) calculation by using the near-infrared (NIR) and red bands (7).

$$NDVI = (NIR - Red)/(NIR + Red) \tag{7}$$

where NIR is the band 5 and Red is the band 4 for the Landsat-8/9.

- The proportion of vegetation coverage (P_v) calculation by NDVI values (8).

$$P_v = ((NDVI - NDVI_{min})/(NDVI_{max} + NDVI_{min}))^2 \tag{8}$$

- Land surface emissivity calculation to scale the blackbody radiance (Planck's law) for emitted radiance prediction (9).

$$e_\lambda = e_{v\,\lambda} * P_v + e_{s\,\lambda}\,(1 - P_v) + C_\lambda (\text{if } NDVI_s <= NDVI <= NDVI_v) \tag{9}$$

where e_v is the vegetation emissivity, e_s is the soil emissivity, and C is the surface roughness (C = 0 for homogenous and flat surfaces).

$$T_s = BT/(1 + (\lambda * BT/p) * ln(e_\lambda)) \quad (p = h * c/q \approx 143.8mK) \tag{10}$$

- The emissivity corrected LST calculation by using BT and e_λ (10).

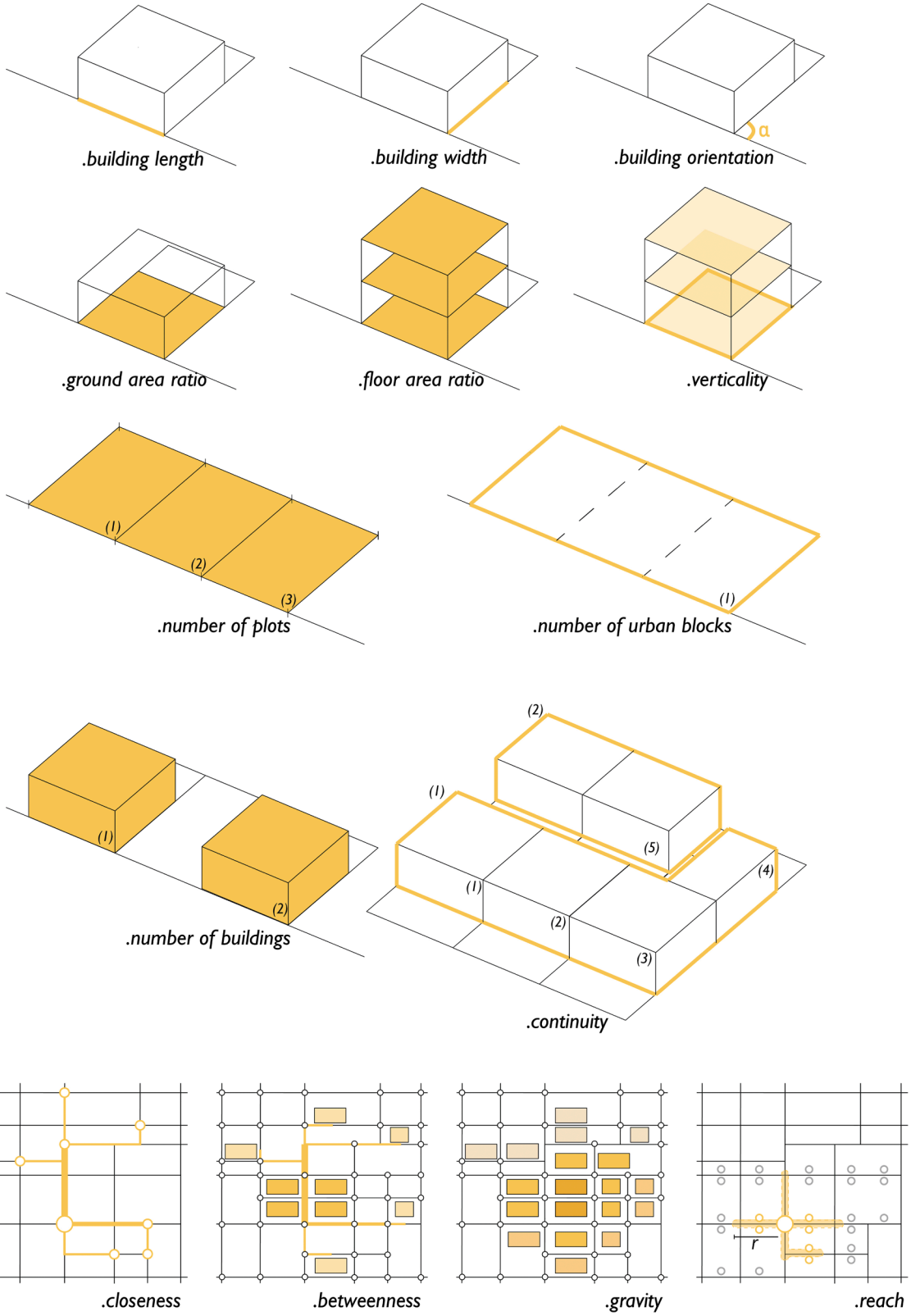

Fig. 2. Morphological variables of the building envelope, plot and urban block. (Small figures include the number of units concerned. α shows the angle of orientation.).

where λ is the wavelength of emitted radiance (for which the peak response and the average of the limiting wavelength (λ≈10.895), q is the Boltzmann constant (1.38×10^{-23} J/K), h is the Planck's constant (6.626×10^{-34} J s), c is the velocity of light (2.998×10^{8} m/s).

- Validation of LST values by in-situ measurements of fixed meteorological stations [64].

Afterwards, the percentage of LST measurement area within the hexagon (P_{index}) was calculated to eliminate the mismatch resulting from the resampled spatial resolution and a shape edge effect of hexagons [65,66]. Employing the P_{index} disables the mismatch of LST pixel sizes in 30 m × 30 m resolution, enables cooperation with the thermal characteristics of the surroundings beyond the boundaries of hexagons and improves the accuracy of the research model. An index value of 1.0 signifies that the shape fully encompasses all the LST pixels, representing the optimal condition within the model. The P_{index} calculation in this research revealed no noteworthy pixel issues ($P_{index} \approx 1.0$ for all hexagons).

2.3. Multi-scale morphological measurement

The research employed fourteen morphological variables to analyse the multi-scale heterogeneity in urban morphological space [67]. These metrics are categorised into four different morphological scales: (1) building, (2) plot, (3) urban block and (4) network (Fig. 2). To perform spatial analyses, each parameter is aggregated on hexagons.

2.3.1. Building – building envelope

To ascertain the impact of various building-level parameters [68] on the research outcome, six of them, *building length, building width, building orientation, number of buildings, verticality, and continuity* were computed. *Building length* (BLL), as one of the fundamental parameters, refers to the longer side of the building. The length of a building, together with the width, serves to define the building's perimeter. This, in turn, influences the spatial configuration of urban fabric. *Building width* (BLW) is the shorter side of the building footprint. It serves as a complementary parameter to building length. Together with building length, it configures the overall dimensions of a building. *The orientation of a building* (BLO) is defined as the angular expression of the direction that the front facade or the main axis of a building faces, measured relative to a fixed reference direction, typically true north. *The number of buildings* (BLC) guides the entire count of individual building units within the hexagon. In urban morphology, the number of buildings indicates urban density, which has significant implications for urban planning and design [69].

The verticality (VER) metric is defined as the ratio between the total height and the footprint area of the building. It is important to note that the verticality of a building can be perceived as a subjective indicator in urban morphology, as the perceived height of a building can vary considerably depending on the surrounding context [69]. However, it can be measured with the mathematical definition:

$$Verticality = \frac{h_j}{Af_j} \tag{11}$$

where h_j is the height of building *j*, Af_j is the total area of the building footprint for building *j*.

The continuity (CON) indicator, related to the grain of the urban fabric [69], basically quantifies the rate of the total count of individual building units to the total number of building envelopes within the urban fabric. Correspondingly, it is formulated as:

$$Continuity = \frac{Nbld}{Nenv} \tag{12}$$

where Nbld is the total number of buildings and Nenv is the total number of envelopes in a given area.

2.3.2. Plot

For the plot, the research calculated two complementary density parameters, *floor area ratio (FAR)* and *ground area ratio (GAR)*, to provide insight into the two- and three-dimensional nature of the built environment. *GAR* is the proportion of the built-up footprint area of a building to the area of the plot where the building is on it [70]. It is calculated as the ratio between the building footprint and the total plot area, formulated as follows:

$$GAR = \frac{Afj}{Aj} \tag{13}$$

where Afj is the coverage (footprint) of the building on plot j, and Aj is the area of plot j. It also represents the overall figure-ground relationship of an urban fabric. *FAR* is defined as the ratio between the total building floor area to the area of the plot. It is quantified as:

$$FAR = \frac{Atfj}{Aj} \tag{14}$$

where Atfj is the total floor area of the buildings on plot j, and Aj is the area of plot j. In another way, it can be calculated by multiplying the GAR by the number of floors. FAR is a significant parameter for the built environment as it correlates with habitable volume density and land use efficiency.

2.3.3. Urban block

Two parameters, the *number of urban blocks* (UBB) and the *number of plots (subdivisions)* (UBP), were calculated to evaluate the relations in an urban block scale. *UBB* refers to the total count of distinct, bounded areas within a given site, typically framed by street patterns or natural boundaries. The parameter is significant to comprehend the built fabric configuration. On the other hand, an urban block consists of several plots, each of which has a distinct size and shape. In this sense, *UBP* explains the total count of individual parcels within the given urban block. Since the number of subdivisions also directly indicates the building density, this parameter also provides information about the granularity of the urban fabric.

2.3.4. Urban network parameters

The research employed the following four network centrality parameters in the analysis; *reach, gravity index, betweenness*, and *closeness* [71]. These measurements are operated to quantify the significance of each node in a network. *The reach* (REA) describes the extent to which a specific point can be accessed from other locations or nodes within a given distance or time threshold. This concept is essential for comprehending the connectivity and accessibility of different areas within an urban environment. The factor can be parametrised as follows:

$$Reach\ [i]^r = \sum_{j \in G-\{i\}; d[i,j] \le r} W[j] \tag{15}$$

where d*[i,j]* is the shortest path distance between origin *i* and destination *j* in graph G, and W*[j]* is the weight of a destination *j*. As originally coined by Hensen [72], *the gravity index* (GRA) is one of the most visited accessibility parameters. In contrast to Reach, Gravity does not merely consider the number of destinations within the specified network radius. Instead, it divides each destination (or destination weight) by the travel cost required to reach it [73]. It is measured as follows:

$$Gravity\ [i]^r = \sum_{j \in G-\{i\}; d[i,j] \le r} \frac{W[j]}{e^{\beta . d[i,j]}} \tag{16}$$

where W*[j]* is the weight of a specific destination *j* that is accessible from *i* within the threshold of radius r. Also, β represents a user-specified exponent that directs the steepness of the distance decay on each shortest path between *i* and *j*. *The betweenness centrality index* (BTW) is a measure of the importance of a node in a network, considering the

frequency with which it appears on the shortest paths between other nodes. A higher value expresses that a node (or building) acts as a significant hub within the urban network [69].

$$Betwenenness[i]^r = \sum_{j \in G-\{i\}; d[i,j] \le r} \frac{n_{jk}.[i]}{n_{jk}}.W[j] \quad (17)$$

The formula serves to quantify the phenomenon [71]. Herein, n_{jk} is the count of the shortest path from node j to node k in G which is the other accessible node. $n_{jk}.[i]$, on the other hand, is the number of those shortest paths that pass-through node i, having j and k in the network with r radius from i. W*[j]* is a weight factor associated with node j. As formulated by Sevtsuk and Mekonnen (2012), *the closeness index* (CLS) is a metric that quantifies the average distance from a specific building to all other buildings in a network. In this way, it allows one to measure, how quickly and easily one can reach other nodes from a given location. It is calculated by employing the following equation, which computes the inverse of the total distance from node i to all other accessible nodes in radius r within graph G.

$$Closeness[i]^r = \frac{1}{\sum_{j \in G-\{i\}; d[i,j] \le r} (d[i,j].W[j])} \quad (18)$$

2.4. Statistical models

Before the statistical models, a multicollinearity diagnostic procedure was conducted to ensure the validity of the predictions and enhance the robustness of the models. The Variance Inflation Factor (VIF) served as a tool for detecting multicollinearity, assessing the increased variance of an estimated regression coefficient when variables are correlated [74,75]. Since residential land use which was kept by eliminating other land use in the hexagon-based sampling step typically has one building per plot, there was a multicollinearity expectation between number of plots (UBP) and building counts (BLC). However, Istanbul's urban fabric has residential plots with more than one building on a single plot. Thus, statistics, values below the VIF threshold 10, showed no strong correlation between UBP, BLC, or other independent variables.

To assess the impact of the independent variables on $LSThex_{mean}$, two statistical models were incorporated into the research: (1) MGWR and (2) XGBoost. Additionally, the research benefited from SHAP analysis to further investigate the black-box nature of the XGBoost by offering insight into the model findings through additional analysis and visuals. Before applying the statistical models, Z-score normalisation was performed on the dataset, ensuring that each feature had a mean of 0 and a standard deviation of 1, thus standardising the data. It is quantified as follows:

$$X_{scaled} = (X - \mu)/\sigma \quad (19)$$

where X is the original value, μ is the mean of the feature, and σ is the standard deviation of the feature.

2.4.1. Multi-scale geographically weighted regression (MGWR)

The research employed MGWR due to its greater flexibility and advanced framework in compared to prior models like GWR. It allows for the spatial relationship analysis between dependent and independent parameters at different spatial scales [76]. This analysis framework provides more significant adaptability for the model that can aid in minimising over-fitting and collinearity, and decreasing bias in parameter estimates [77]. In this context, the MGWR is quantified as follows [28]:

$$y_i = \beta_0(u_i,\ v_i) + \sum_{j=1}^{p} \beta_j(ui,\ vi)x_{ij} + \varepsilon_i \quad (20)$$

where $\beta_0(u_i, vi)$ represents the local intercept of the i th observation, β_j $(u_i,\ v_i)$ denotes the parameter associated with the j-th independent variable x_{ij}. Finally, ε_i symbolises the random error term, and $(u_i,\ v_i)$ displays the spatial coordinates of the i th observation. The MWGR model utilised the LST as the dependent variable and the fourteen morphology and network indicators as the independent variable.

The model outputs coefficient statistics to build the linear function and interpret results better. The *mean coefficients* capture the average influence of each independent variable across all spatial locations, assuming stable and consistent relationships between dependent and independent variables, making them suitable for generalising effects through a uniform equation applicable across the study area. The *standard deviation* provides insight into the variability of coefficients across spatial locations, emphasising the extent to which relationships between dependent and independent variables differ regionally. It quantifies uncertainty and spatial variability, offering a measure of how the model's behaviour fluctuates across different areas. Mean coefficients are appropriate for constructing the final MGWR function, offering a simplified and generalisable equation for making predictions uniformly across all spatial locations. The model also computes the model accuracy by employing three different parameters: (1) the coefficient of determination (R^2), (2) the adjusted coefficient of determination (Adj. R^2), and (3) the root mean square error (RMSE).

2.4.2. eXtreme gradient boosting (XGBoost) and shap analysis: understanding the black-box

XGBoost, a novel approach, utilises a series of decision trees to provide accurate predictions, ensures a robust ground for preventing overfitting, and missing value handling, and supports parallel and distributed computing. It is a widely used method for quantifying the relationship between urban spatial features and land surface temperature [78–81]. In this context, this research run XGBoost with LST as the dependent variable and the fourteen morphology and network indicators as independent variables. To train the XGBoost model, the sample data were divided into training and validation sets. Subsequently, SHAP (SHapley Additive exPlanations) scores were computed to interpret the model's predictions, as they provide clear insight into how each variable affects the model's output. The model computes the model accuracy by employing three different parameters: (1) the coefficient of determination (R^2), (2) the adjusted coefficient of determination (Adj. R^2), and (3) the root mean square error (RMSE).

The SHAP method, utilised in this research to better explain the XGBoost model results, provides quite useful ground to explicate and interpret the prediction of the model. It has proven success [4,81] in demonstrating the importance of several variables to the urban heat island. In this sense, the research introduced the additive feature attribution method [38]. The method propounds the prediction of a model, expressed $g(z')$, as a sum of contributions derived from each variable. This is formulated as follows:

$$g(z') = \varnothing_0 + \sum_{i=1}^{M} \varnothing_i z_i' \quad (21)$$

where, $\varnothing_0$, as a base value, expresses the average estimation within the entire dataset and $\varnothing_i$ is a SHAP value that indicates the contribution of variable i to the prediction, quantifying how much this feature increases or decreases the predicted value. z_i' is a binary indicator that shows whether feature i is present (1) or absent (0) in the specific instance being explained and M represents the total number of variables in the model that are used to make predictions.

To conclude the model explanation, the research also computed the SHAP [82]. The SHAP value for the selected variables demonstrates the average contribution of that variable among every possible subset of combinations for the variable. It is calculated as follows:

$$\varnothing_i = \sum_{S \subseteq N \setminus \{i\}} \frac{|S|!(|M| - |S| - 1)!}{|M|!} [f_x(S \bigcup \{i\}) - f_x(S)] \quad (22)$$

where S is the total number of variables, N\{i} is a set of all possible combinations of variables, S is a feature set in N\{i}, $f(S)$ is the model prediction with variables in S, and $f(S \cup \{i\})$ is the model prediction with variables in S. SHAP is a crucial approach in the explanation the rationale behind XGBoost models, offering a comprehensive understanding of the influence of individual features on model predictions, ensuring both accuracy and transparency. In this research, SHAP values assist in understanding the impact of urban morphology and network variables on LST, thereby providing a more comprehensive picture of the model.

2.5. Sensitivity analyses

The study employed sensitivity analyses using Monte Carlo simulation and Tornado Diagram for MGWR and SHAP scores for XGBoost to assess how the uncertainty in model outputs can be attributed to various sources of uncertainty in the model's input parameters. Sensitivity analyses demonstrated the impact of varying independent variable values on a dependent variable, within the constraints of a specified set of assumptions.

2.5.1. Monte Carlo simulation for MGWR

Monte Carlo simulation is a widely used method for sensitivity analysis in machine learning [5,83] allowing models to respond to randomly generated inputs through a resampling approach. In this research, 10.000 design scenarios were generated with varying quantitative combinations of normalised independent variables. The model estimated the distribution of random variables and assessed the model's stability and robustness, particularly the sensitivity of the model output (LST_{mean}) to changes in independent variables. Measures of central tendency, variability, skewness, and kurtosis were analysed to evaluate the dataset, while a Sensitivity Tornado Plot assessed the impact of independent variables on temperature variations.

2.5.2. SHAP scores for XGBoost

The research operated the sensitivity analysis on the XGBoost model by using SHAP values to understand feature importance and perturbing features to observe changes in model predictions for $LSThex_{mean}$. This sensitivity analysis aims to reveal the influence of each parameter on the output of the model and the identification of the most impactful parameters. The research used a 10 % perturbation factor to perform sensitivity analysis.

3. Results

3.1. Urban heat heterogeneity in Istanbul

In Istanbul, land surface characteristics are divided between natural landscapes in the north and urbanised areas in the south and along the Bosphorus shores. The land surface temperatures in 2023 followed this north-south division and tended to increase towards the south. The only overheated area in the European north, the Istanbul Airport, has led to the degradation of forestry-water lands and induced a warming trend towards the northern natural areas, with the airport exhibiting temperature levels comparable to urbanised regions (Fig. 3).

The quantitative results of Istanbul's LST demonstrated a significant increase and a clear overheating trend in the city since LST_{max} was around 51 °C in 2023, but 48 °C in 2021 [65]. Moreover, LST_{mean}, around 34 °C, was almost 10 °C higher than the long-term average (25.5 °C in July) [42]. The findings indicated that 51 % of Istanbul has an average temperature of 37.01 °C, which is 3 °C higher than the LST_{mean}. Istanbul's urban landscape also offered hotspot urban fabrics in which temperature exceeds the LST_{mean} up to 6 °C.

The heterogeneous urban landscape of Istanbul demonstrated discrete surface temperature patterns in the metropolitan area (Fig. 3). Proxies of Istanbul's urban area, hexagon units, indicated an urban heat heterogeneity with a temperature range between 33 and 43 °C. The $LSThex_{mean}$ was around 39 °C, 5 °C above the LST_{mean} (Table 1). The results showed that 3 % of hexagon units experience temperature anomalies above LST_{mean} by 1 °C, 9 % by 2 °C, 11 % by 3 °C, 14 % by 4 °C, 17 % by 5 °C, and 45 % by 6 °C or more. A notable level of spatial variability in $LSThex_{mean}$ was observed even among adjacent hexagon units.

3.2. Spatial heterogeneity of morphological features

The research investigated fourteen morphological variables in four categories: building, plot, urban block and urban network. The analysis of the spatial heterogeneity of morphological parameters revealed significant variability across Istanbul, as evidenced by the descriptive statistics for each variable (Table 1). To establish a balanced overview of the statistical distribution of the variables, the research normalised all morphological parameters, illustrating the distribution pattern with the box plot (Fig. 4).

Providing significant local variability, the building-level parameters and indicators exhibited different statistical distributions (Table 1). Accordingly, BLC had a mean of 119.46 with a substantial standard deviation (SD) of 82.86, indicating a wide range from 2 to 565 buildings. BLW, with a mean of 17.76 and an SD of 7.38, showed moderate variability with values ranging from 9.29 to 66.36. Similarly, BLL, which had a mean of 11.41 and an SD of 3.61, ranged from 5.77 to 41.34. BLO and VER also exhibited spatial heterogeneity. BLO had a mean of 89.1° and an SD of 21.75, with values ranging from 24.53 to 152.9. VER, with a mean of 0.14 and an SD of 0.06, ranged from 0.01 to 0.42, reflecting notable variability. CON, with a mean of 2.22 and an SD of 1.81, ranged from 0.92 to 16, indicating significant variability.

FAR and GAR, both plot parameters, demonstrated moderate to broad spatial heterogeneity. GAR had a mean of 0.32 and an SD of 0.14, ranging from 0.1 to 0.72. FAR showed a mean of 1.33 and an SD of 0.82, ranging from 0.16 to 7.44. Among urban block parameters, UBP showed a mean of 111.76 and an SD of 93.81, ranging from 1 to 615. UBB, with a mean of 20.86 and an SD of 13.46, ranged from 1 to 104 indicating widespread influence. Both urban block parameters indicated moderate spatial variability.

Urban network parameters demonstrated a mix of consistent and extensive influences. Among the parameters, REA had a mean of 19.51 and an SD of 16.87, ranging from 0 to 181.48, indicating a consistent distribution across the research area. BTW, with a mean of 217.26 and an SD of 439, ranged from 0 to 7528.39, showing significantly lower spatial heterogeneity. CLS, with a mean of 0.01 and an SD of 0.04, ranged from 0 to 0.87, also suggesting limited variability. Representing diverse spatial heterogeneity, GRA had a mean of 0.1 and an SD of 0.08, ranging from 0 to 0.5.

3.3. MGWR results

To assess the performance of the model, the research utilised four metrics: the R-squared value (R^2), the adjusted R-squared value (adj. R^2), the corrected Akaike information criterion (AICc), and the sigma-squared (SS). The R^2 indicated that the MGWR model explains approximately 88 % of the variability in $LSThex_{mean}$, which revealed that the independent parameters are highly relevant to $LSThex_{mean}$. Furthermore, the adj. R^2 value of 0.86 validated the goodness of fit of the model, indicating that the model remains robust even after adjusting for the degrees of freedom. A relatively low AICc, 1061.96, indicated that the model exhibits an optimal balance between the model complexity and goodness of fit. This meant a significant aspect of avoiding overfitting while keeping the model statistically meaningful. The SS value of 0.13 provided further evidence of the model's accuracy. It represented the variance of the residuals and indicated that the model's predictions were close to the observed values (Table 2).

The model provided the mean coefficient values of morphological

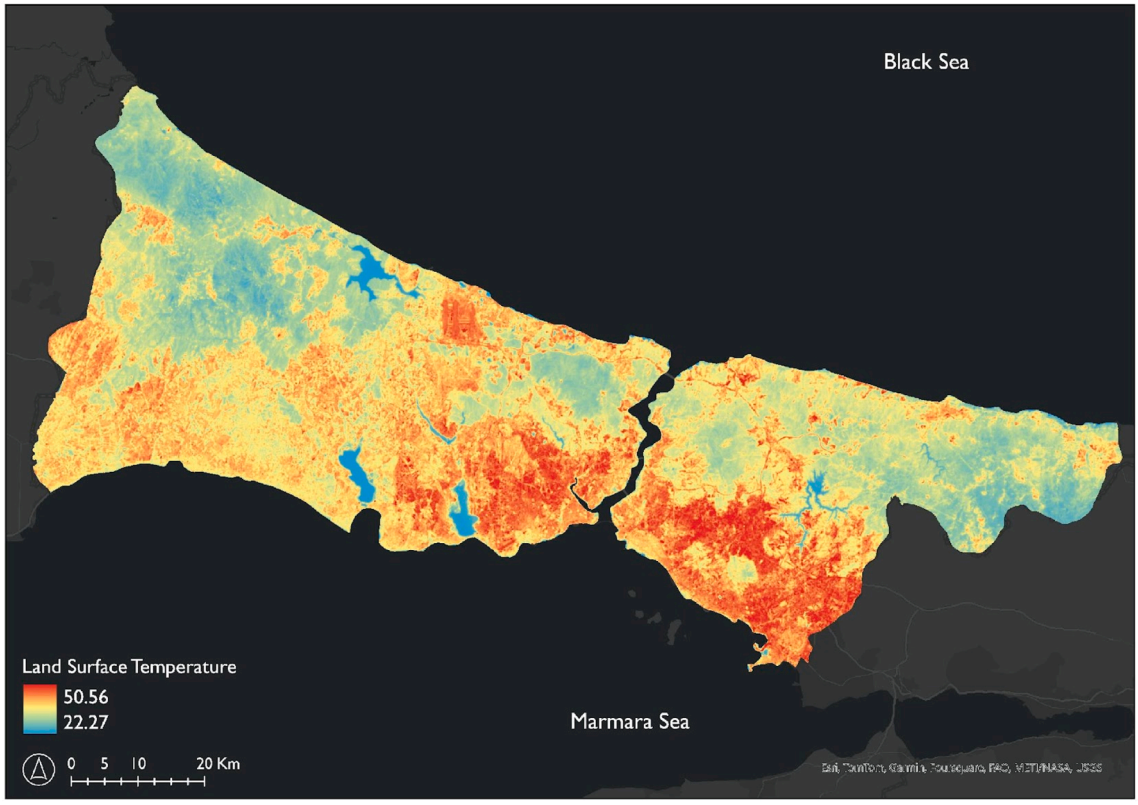

(a)

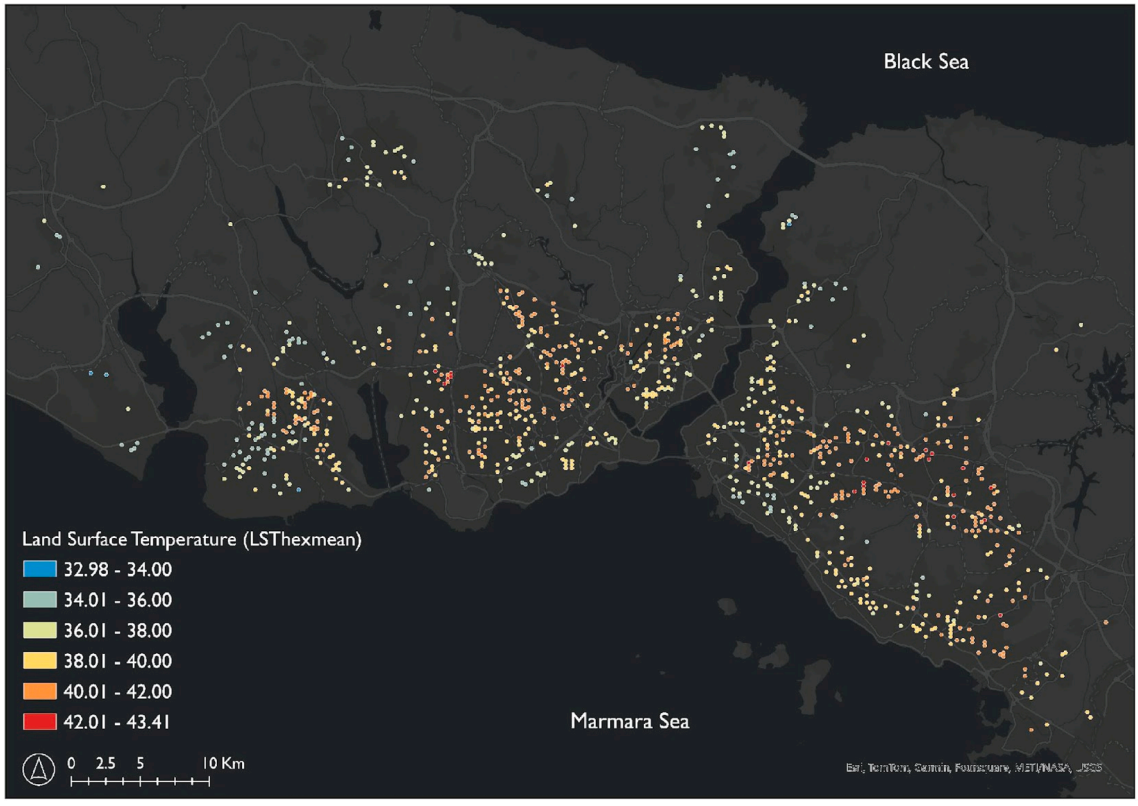

(b)

Fig. 3. Urban heat distribution in Istanbul on 26th July 2023. (a) LST map (b) the LST_{mean} values in hexagon units.

Table 1
Descriptive statistics of morphological features.

Variables (n = 981)	Unit	Variable Code	Mean	SD	Median	Min	Max
Dependent Variable							
Land Surface Temperature	°C	$LSThex_{mean}$	38.83	3.27	39.09	32.98	43.41
Independent Variables							
Building Parameters							
Building Count	number	BLC	119.46	82.86	102	2	565
Building Width	meter	BLW	17.76	7.38	15.26	9.29	66.36
Building Length	meter	BLL	11.41	3.61	10.39	5.77	41.34
Building Orientation	degree	BLO	89.10	21.75	88.86	24.53	152.9
Verticality	–	VER	0.14	0.06	0.14	0.01	0.42
Continuity	–	CON	2.22	1.81	1.52	0.92	16
Plot Parameters							
Ground Area Ratio	–	GAR	0.32	0.14	0.31	0.10	0.72
Floor Area Ratio	–	FAR	1.33	0.82	1.23	0.16	7.44
Urban Block Parameters							
Number of Plots	number	UBP	111.76	93.81	92	1	615
Number of Urban Blocks	number	UBB	20.86	13.46	18	1	104
Network Parameters							
Reach	–	REA	19.51	16.87	15.33	0	181.48
Betweenness	–	BTW	217.26	439	90.16	0	7528.39
Closeness	–	CLS	0.01	0.04	0	0	0.87
Gravity	–	GRA	0.10	0.08	0.10	0	0.50

- variables without any dimension.
SD: Standard deviation.

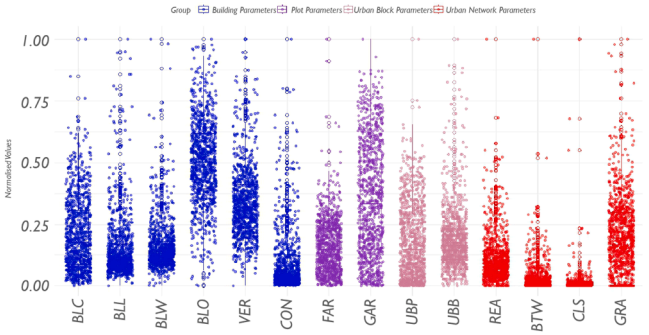

Fig. 4. Box plot of the morphological parameters based on normalised values. (BLC: Building count, BLL: Building length, BLW: Building width, BLO: Building orientation, VER: Verticality, CON: Continuity, FAR: Floor area ratio, GAR: Ground area ratio, UBP: Number of plots, UBB: Number of blocks, REA: Reach, BTW: Betweenness, CLS: Closeness, GRA: Gravity).

features, quantifying the average effect and impact direction of each one on the urban heat (Table 2). In this case, the fitted MGWR function for $LSThex_{mean}$ predictions in Istanbul's urban fabrics are as follows ($\in$ is the error term in the model):

$$\begin{aligned} LSThex_{mean} = {} & 0.0906 - 0.0746 * BLC - 0.0462 * BLL - 0.0153 * BLW \\ & - 0.0112 * BLO - 0.0779 * VER + 0.0799 * CON + 0.5603 \\ & * GAR - 0.1064 * FAR + 0.2140 * UBP + 0.0315 * UBB \\ & - 0.0579 * BTW + 0.0129 * CLS + 0.0085 * GRA + 0.0256 \\ & * REA + \in \end{aligned} \quad (23)$$

Results implied strong positive correlations of GAR (coefficient: 0.56), and UBP (coefficient: 0.21) with $LSThex_{mean}$, which means the dominant impact of plot and urban block variables creates a warming trend with an increase in values. FAR (coefficient: −0.11), the other plot parameter, also had a dominant impact on LST variations, but in a negative direction which means higher vertical density created lower temperatures in Istanbul's urban fabric. CON (coefficient: 0.08) was on the 4th raw in the overall impact on $LSThex_{mean}$. It had not only the highest impact but also was the only one positively correlated among the building parameters. Hereafter, the impact level ranged as VER, BLC, BLL, BLW, and BLO in building scale. They showed negative correlations with the $LSThex_{mean}$ and indicated a strong potential for heat mitigation in urban morpho-space by features related to the building granularity. Among the network parameters, BTW (coefficient: −0.06) was the most influential variable and the only one with a negative correlation with $LSThex_{mean}$. It was followed by REA, CLS and GRA which had an impact on increasing the $LSThex_{mean}$ with a positive correlation to the urban heat (Figs. 5, 6).

The standard deviation and the difference between maximum and minimum values of explanatory variables indicated the level of spatial variability of related variables whether is consistent in the global scale of Istanbul or has a local impact on the urban fabric. Among the multiscale morphological nature of buildings, plots, urban blocks, and networks, building parameters - BLC, CON, VER, and BLL - had the highest spatial variability in Istanbul, which shows a higher local value on urban heat in topological sub-regions. However, BLO and BLW demonstrated more global impact among the building parameters with relatively lower standard deviation values. Due to Istanbul's topographical structure, buildings traditionally tend to be located with consistent orientation and width features (Fig. A.1).

In the overall model, GAR (std.: 0.002) emphasised a consistently strong positive influence on $LSThex_{mean}$ throughout Istanbul, with minimal spatial variability. However, the higher spatial variability of the FAR (std.: 0.03) signalled that the strong global negative influence may tend to differentiate in some topological sub-regions. Nevertheless, the lower spatial variability of FAR among overall model variables constructs it more consistent in creating a mitigation impact on LST (Figs. 5, 6).

Among the urban block parameters, UBP (std.: 0.08) had higher spatial variability than the UBB (std.: 0.003) but was lower than the building parameters. In residential areas, the context of this research, while the number of plots may vary to the topological sub-regions, typically a single building exists on a single plot, and the number of blocks remains constant. However, since Istanbul's residential characteristic hosts more than one building on a single plot in particular topological sub-regions, the spatial variability of UBB remained at a medium level and negligible compared to other variables. Therefore, the positive influence of both urban block parameters is consistent locally and globally in Istanbul's urban landscape. Higher values of UBP and UBB create a tendency for higher urban temperatures (Figs. 5, 6).

In the urban network parameters, REA (std.: 0.001) and CLS (std.:

Table 2
Summary statistics for MGWR model results and coefficients estimates.

Statistics				MGWR		
R-Squared				0.88		
Adjusted R-Squared				0.86		
AICc				1061.96		
Sigma-Squared				0.13		
RMSE				0.37		
Explanatory Variables	Mean	Standard Deviation	Minimum	Median	Maximum	Neighbours (% of Features) *
Intercept (Scaled)	0.0906	0.5924	−1.0915	0.0116	1.5913	30 (3.06)
BLC	−0.0746	0.1199	−0.3287	−0.0784	0.2860	88 (8.97)
BLL	−0.0462	0.0756	−0.1896	−0.0704	0.2067	123 (12.54)
BLW	−0.0153	0.0033	−0.0203	−0.0156	−0.0098	981 (100.00)
BLO	−0.0112	0.0039	−0.0162	−0.0123	−0.0024	981 (100.00)
VER	−0.0779	0.1025	−0.3007	−0.0817	0.2734	60 (6.12)
CON	0.0799	0.1406	−0.1705	0.0377	0.4326	144 (14.68)
GAR	0.5603	0.0024	0.5566	0.5602	0.5655	981 (100.00)
FAR	−0.1064	0.0318	−0.1454	−0.1134	−0.0564	671 (68.40)
UBP	0.2140	0.0817	0.0627	0.2055	0.3671	360 (36.70)
UBB	0.0315	0.0038	0.0264	0.0320	0.0376	981 (100.00)
BTW	−0.0579	0.0620	−0.2058	−0.0299	0.0035	426 (43.43)
CLS	0.0129	0.0022	0.0085	0.0135	0.0165	981 (100.00)
GRA	0.0085	0.0116	−0.0053	0.0052	0.0306	842 (85.83)
REA	0.0256	0.0011	0.0237	0.0257	0.0278	981 (100.00)

* This number in the parenthesis ranges from 0 to 100 %, and can be interpreted as a local, regional, or global scale based on the geographical context from low to high.

0.002) demonstrated the highest consistency across the model, whereas BTW (std.: 0.06) and GRA (std.: 0.01) exhibited moderate to negligible spatial variability. Consequently, while REA and CLS consistently exerted positive influences across Istanbul, the negative influence of BTW was more localised. Overall, increases in network variable values corresponded with a consistent positive correlation to rising LST. Specifically, as reach, closeness, and gravity values increased, a concomitant increase in LST was observed.

3.4. SHAP-explained XGBoost results

XGBoost demonstrated robust predictive capability for urban heat, achieving an R-squared value of 0.56, indicating that the model explains 56 % of the variance in the LST heterogeneity. The adj. R-squared value of 0.53 accounts for the complexity of the model and confirms a moderate fit to the data by incorporating multi-scale morphological features of buildings, plots, urban blocks, and networks. The model's RMSE of 1.20 suggests that, on average, the predictions deviate from the actual values by approximately 1.20 units. These validation results demonstrate a reasonable predictive performance, with the SHAP analysis providing a valuable understanding of feature contributions and their interpretability (Table 3).

Gain, cover and weight are primary outputs to evaluate the feature importance in the XGBoost model. Gain values quantified the contribution of features to the model accuracy by assessing their effectiveness in data splitting at each node, with higher gain values indicating greater importance in reducing the loss function and enhancing the predictive power of the model. Cover assessed the influence of the features on the number of observations, providing insight into the proportion of data affected by their splits; a high cover value signified that the feature frequently impacts a substantial portion of the data. Weight signified the frequency with which the features split data in the model's decision trees; a higher frequency indicated the feature was crucial in reducing the loss function. The metric offered a clear understanding of feature importance by revealing how often each feature guides decision-making in the trees, thus identifying those most utilised.

Given the morphological features in the model, GAR, UBP, BLC, and CON exhibited notably higher gain values and feature importance, which was highly consistent with MGWR results. While FAR had relatively lower feature importance, urban network parameters distinctively indicated the least feature importance values in XGBoost model results. The cover values of features in the model showed that GAR, BLC, and VER are of relatively higher importance. According to the weight values, BLC had higher feature importance which emphasises the dominant impact of building scale on urban heat heterogeneity (Table 3).

The contributions of urban morphological features on urban heat were assessed by global (Fig. 7a) and local explanations (Fig. 7b) of SHAP values. Fig. 7a ranked the global contributions of features on urban heat from the top (the highest contribution) to down (the lowest contribution). Accordingly, a plot parameter, GAR, had the highest contribution to the model and was respectively followed by UBP, BLC, CON, and FAR. The least global contributions were from CLS, REA, BTW, BLL, and GRA. Urban network parameters exhibited a relatively low impact on urban heat globally, and the building length (BLL) was similarly included in the feature set with minimal influence. According to global explanations, BLC was the highest and BLL was the lowest contributor among building parameters, while GRA was the highest and CLS was the lowest in network parameters (Fig. 7a).

A SHAP beeswarm plot (Fig. 7b) summarised the local importance and the effects of all features in the model. Local explanations with the beeswarm plot demonstrated the feature importance based on individual SHAP scores, the horizontal distribution to understand how much the SHAP values vary for different datasets, and the correlation directions of morphological features. GAR made a significantly higher contribution than other variables, with a contribution level of 65 %. It was followed by UBP at 37 %, BLC at 26 %, CON at 20 %, and FAR at 19 %. In the third group, there were UBB and VER with contribution values of 13 %, and BLO and BLW with 12 %. The least contributing ones were GRA with 7 %, BLL with 6 %, BTW with 5 %, and REA and CLS with 3 % for each. Network parameters and building length again exhibited a relatively low impact on urban heat at the local level. Local explanations indicated that BLC is the highest and BLL is the lowest contributor in building parameters, while GRA is the highest and CLS is the lowest contributor among urban network parameters, consistent with global explanations (Fig. 7b).

The SHAP dependence plot showed the relationship between a single morphological feature and the SHAP values of that feature across the dataset (Fig. 8). The plot indicated the SHAP values of a specific morphological feature on the y-axis and the feature values (independent variable) on the x-axis. The value on the Y-axis stood for the effect of the

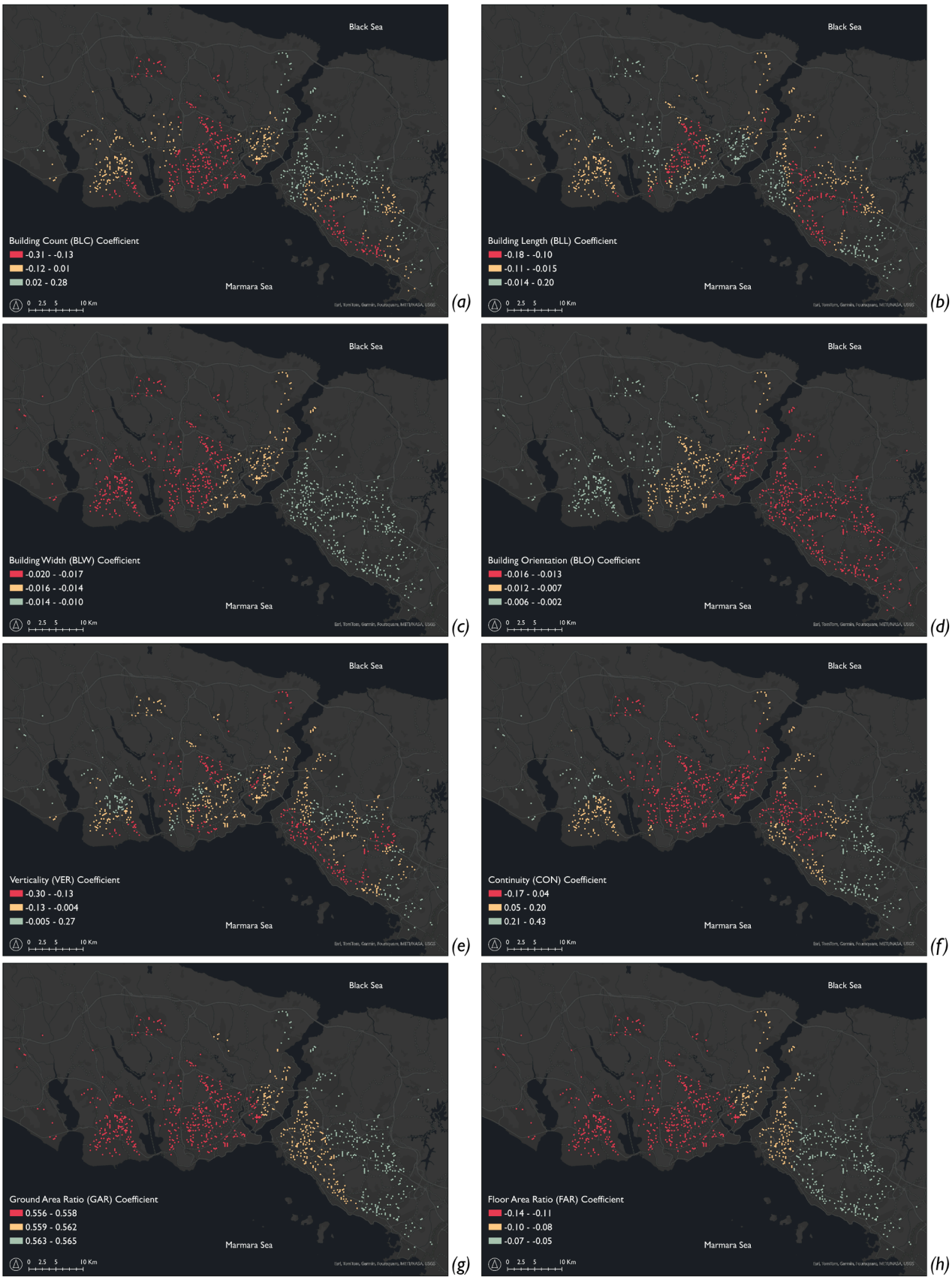

Fig. 5. Spatial distribution of variable coefficients for MGWR-I. BLC(a), BLW(b), BLL(c), BLO(d), VER(e), CON(f), GAR(g), FAR(h).

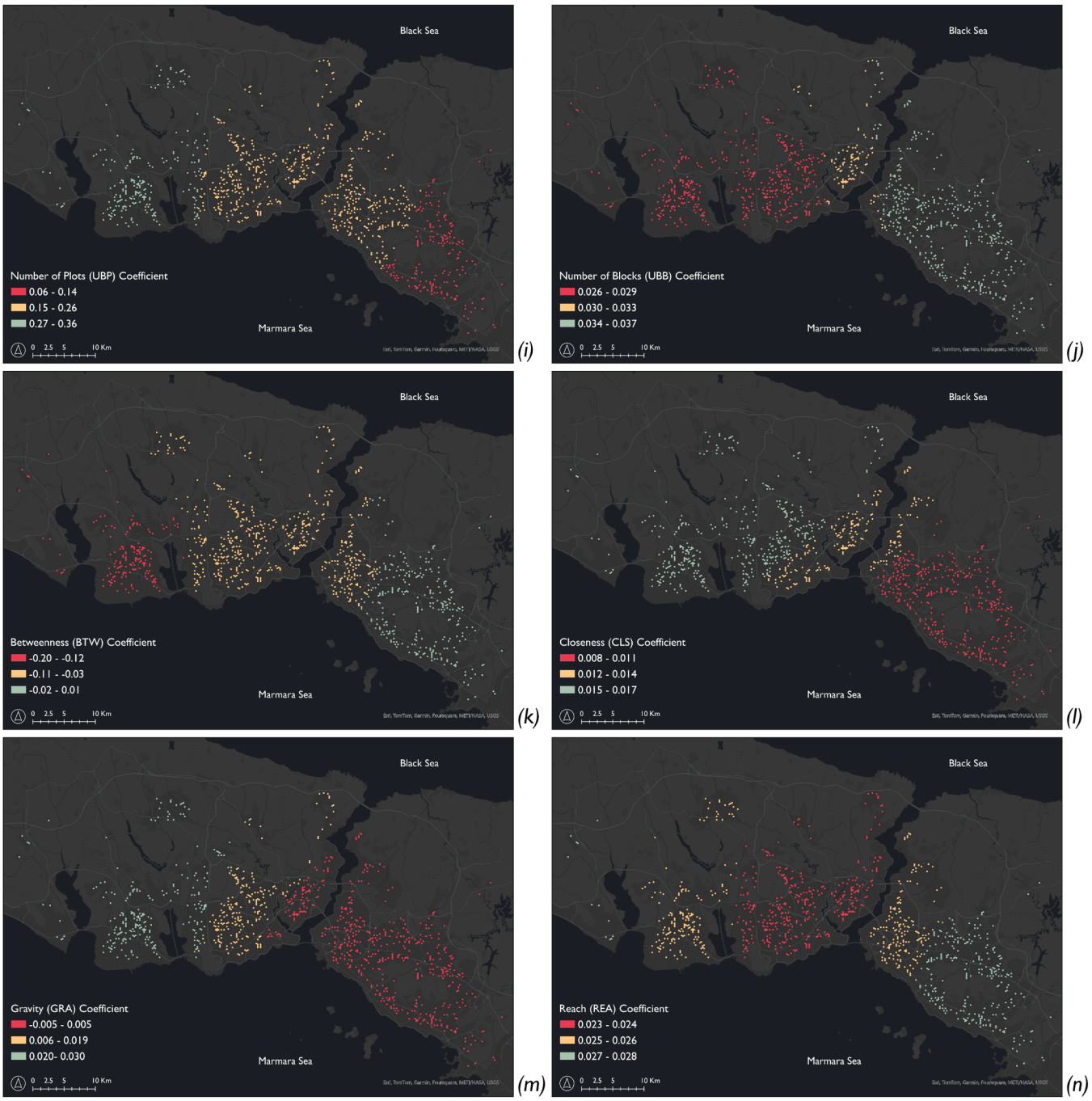

Fig. 6. Spatial distribution of variable coefficients for MGWR-II. UBP(i), UBB(j), BTW(k), CLS(l), GRA(m), REA(n).

feature on $LSThex_{mean}$. The plot revealed how changes in the feature value affect the prediction. The SHAP value in the plot also exhibited the inflection zones where there is a change in direction or slope to indicate when the relationship between the feature value and urban heat shifts from linear (steady increase or decrease) to non-linear (i.e., levelling off, reversing direction, or showing diminishing/increasing returns).

According to the plots in Fig. 8, CON and REA showed more linear behaviour, suggesting a straightforward relationship with urban heat, where changes in the feature values have a consistent impact on the model output. CON exhibited a linear trend, with increased continuity leading to a consistent reduction in urban heat, likely due to enhanced airflow or shading, while REA demonstrated a steady rise in heat levels as urban areas became more accessible. On the other hand, GAR, UBP, FAR, BLC, BLO, VER, UBB, BLL, BLW, GRA, BTW, and CLS exhibited non-linear patterns, indicating that their impact on urban heat is context-dependent and complex.

Accordingly, GAR showed a strong non-linear influence on urban heat. There was a sharp increase in heat at low values of GAR, which suggests that increasing the ground area ratio dramatically increases heat at lower levels, but the effect diminishes as the ratio increases further. The non-linearity of UBP showed an upward trend initially, meaning more plots increase heat. However, the SHAP values flattened out at the inflection point, suggesting a diminishing return - a downward trend in heating or an upward trend in cooling - at a higher number of plots. The U-shaped curve in the SHAP plot for FAR indicated a clear non-linear relationship with LST that both very low and very high FAR values lead to reductions in urban heat, with intermediate values contributing more to heat.

Table 3
SHAP-explained XGBoost model results.

Statistic		XGBoost			
R-Squared		0.56			
Adjusted R-Squared		0.53			
RMSE		1.20			
Independent Variables		Model Performances			SHAP Scores
		Gain	Cover	Weight	
Building	BLC	0.14	0.10	0.15	0.27
	BLW	0.04	0.06	0.06	0.12
	BLL	0.04	0.06	0.08	0.06
	BLO	0.06	0.08	0.09	0.12
	VER	0.06	0.10	0.09	0.13
	CON	0.12	0.09	0.08	0.20
Plot	FAR	0.08	0.09	0.07	0.19
	GAR	0.16	0.12	0.08	0.65
Urban Block	UBP	0.15	0.07	0.07	0.37
	UBB	0.05	0.06	0.06	0.13
Network	REA	0.02	0.03	0.2	0.03
	BTW	0.03	0.06	0.06	0.05
	CLS	0.02	0.04	0.06	0.03
	GRA	0.04	0.04	0.06	0.07

The relationship between BLC and urban heat also demonstrated a distinct non-linear pattern. Initially, as the building count rose, SHAP values increased, indicating a rise in urban heat. However, after reaching the inflection point, this trend stabilised, reflecting a diminishing return effect, which suggests that while the building count significantly influences heat at lower levels, its impact saturates at higher levels, making the relationship non-linear. Similarly, BLO showed varying impacts on urban heat as building orientation shifts, indicating that building orientation affects heat depending on specific configurations and surrounding conditions, leading to a complex, non-linear influence. VER displayed a consistent non-linear and negative trend, where increased verticality initially reduces urban heat, though variability at higher verticality levels makes the relationship less predictable. BLW initially contributed negatively to urban heat, but extreme building widths showed a slight warming effect, reflecting complex interactions with building layout or open space. BLL had an inverse effect, with shorter building lengths cooling the environment, but longer buildings leading to warming, indicating a non-straightforward relationship.

Among the network parameters, GRA also showed a sharp increase in SHAP values at lower values, levelling off at higher values. BTW followed a concave curve, where intermediate values reduce heat, while extreme high or low values increase it. Lastly, CLS exhibited a highly non-linear U-shaped curve, where lower values contribute to cooling, but very high closeness results in a slight warming effect.

3.5. Monte Carlo simulation results

The Monte Carlo Simulation, conducted to assess the sensitivity of the MGWR results, revealed that the distribution of the simulated dataset closely aligns with the training dataset derived from 981 sample hexagons (Table B.1). The histogram confirmed the normal distribution of this test dataset, a critical factor in evaluating the robustness of parametric estimation models. Additionally, the box-and-whisker plot illustrated descriptive values of the simulated dataset, highlighting its variability. Despite a few outliers, the dataset's overall spread, as indicated by the box length, remained consistent for each variable (Figs. A.2, A.3)

The tornado diagram confirmed the MGWR results in terms of the significance and direction of influence (positive or negative) of the independent variables at a 95 % confidence interval (Fig. 9). According to the diagram, GAR and UBP emerged as the strongest, positively correlated contributors, while BLO and GRA had the least influence on the prediction model. The analysis reveals that $LSThex_{mean}$ values were more sensitive to variations in GAR and UBP than other morphological features. CON was also identified as having a significant positive effect on $LSThex_{mean}$, while variables like BTW, FAR, VER, and BLC exhibited a relatively high impact on urban heat but in a negative direction. The only discrepancy between the MGWR results and the Tornado Diagram was the significance of BTW; although MGWR indicated a lower impact, the Tornado Plot demonstrated a higher model sensitivity to BTW (Fig. 9).

3.6. Sensitivity of XGBoost results

Sensitivity analysis for XGBoost focused on how much predictions change when a particular feature is varied, holding other features constant. It highlighted the model's responsiveness to individual features and proved those with the greatest short-term impact on predictions. Sensitivity analysis and SHAP values differed because sensitivity focuses on the immediate impact of changing individual features while holding others constant, highlighting short-term responsiveness. SHAP values, however, provided a holistic view of feature importance by considering the average contribution of each feature across the entire dataset, accounting for interactions between features.

In this sense, the sensitivity analysis revealed that $LSThex_{mean}$ is highly responsive to changes in several key parameters. CON and FAR

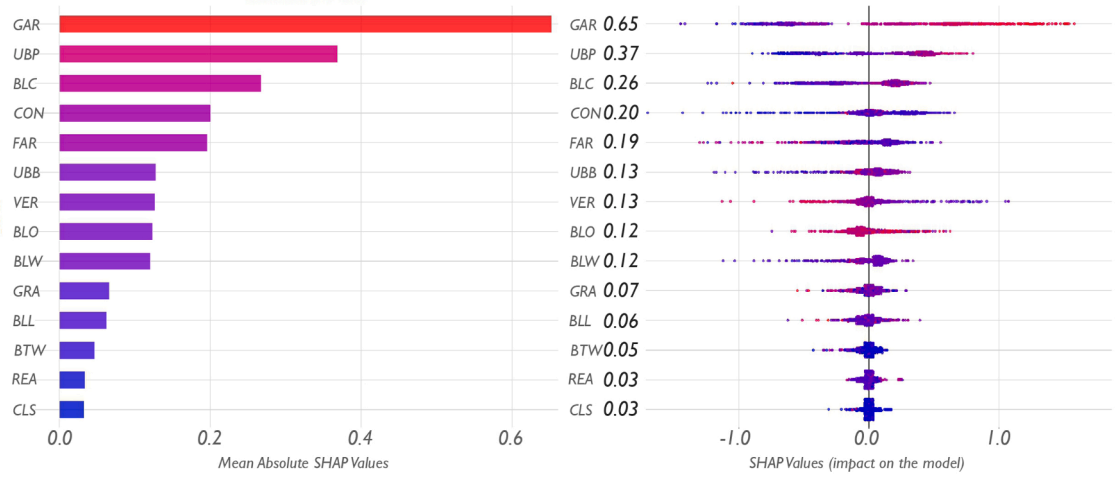

Fig. 7. SHAP values of multi-scale urban morphological metrics. (a-left) The graph of global feature importance, and (b-right) the beeswarm plot of local contributions of metrics on urban heat heterogeneity.

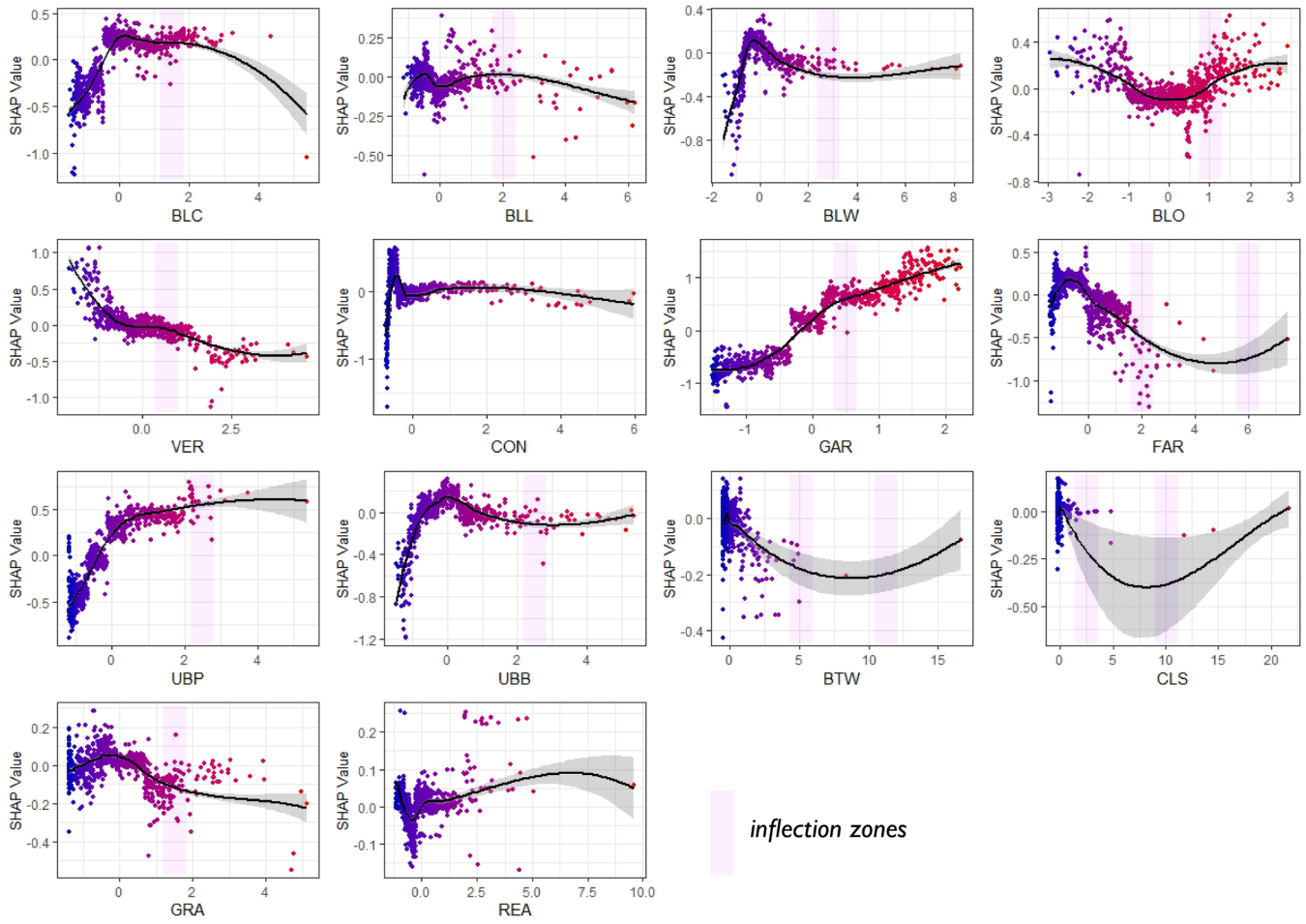

Fig. 8. SHAP dependence plot of multi-scale urban morphological metrics (the purple frame shows the rough inflection zones for each variable).

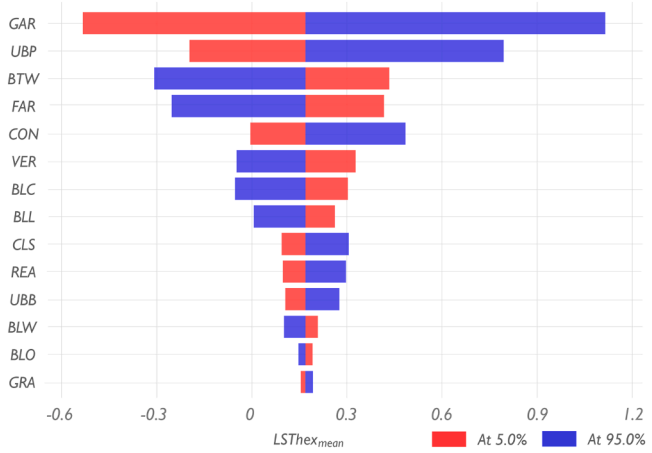

Fig. 9. Sensitivity Tornado Plot.

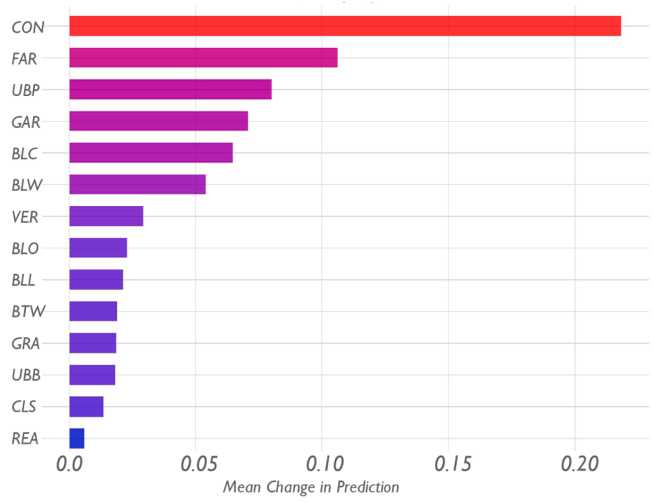

Fig. 10. Sensitivity of the model to the morphological features.

demonstrate the greatest sensitivity, indicating that variations in these parameters cause the most significant shifts in $LSThex_{mean}$ values. This highlighted the strong influence of urban connectivity and building density on surface temperature predictions. GAR and UBP also show considerable sensitivity, suggesting that changes in footprint coverage and plot density significantly affect $LSThex_{mean}$. Building scale parameters, such as BLC, BLW, and BLL, exhibited moderate sensitivity, implying that $LSThex_{mean}$ is influenced by the geometry of buildings, though to a lesser extent than connectivity and density factors. Parameters such as BLO and VER displayed lower sensitivity, meaning $LSThex_{mean}$ is less affected by these features. Network-related variables like BTW, CLS, and GRA exhibited the least sensitivity, indicating minimal impact on $LSThex_{mean}$ (Fig. 10).

4. Discussion

The research employed a comparative framework of conventional linear – MGWR – and advanced ML-based non-linear – XGBoost – statistical models to quantify the influence of multi-scale morphological features on urban heat heterogeneity, discuss the optimal model for capturing the complexity of urban landscapes and explain the cooling benefits associated with the urban morphology and spatial heterogeneity of urban heat. The frame facilitated the exploration of knowledge gaps concerning model-specificity, focusing on the varying performances of statistical models, assessments of building granularity and urban networks, the impact of spatial heterogeneity in linear models, and the interpretability challenges in machine learning outputs. The discussion proceeds by evaluating models' performances, analysing feature importance and contributions, examining coefficient directions, and assessing morphological features' warming or cooling impacts on urban LST.

Global performances of both models showed that the MGWR model demonstrates higher predictive power with 0.86 adj. R^2 value than XGBoost with 0.53. MGWR also had higher predictive accuracy and lower root mean squared error compared to the XGBoost model. However, spatial statistical models like MGWR, while effective under their specific assumptions, may struggle with complex data processes, overlook non-linear effects, and result in biases. Therefore, despite the relatively lower prediction level, ML is more advantageous and robust with fewer assumptions [4,84,85]. Moreover, XGBoost is more adept at modelling discrete spatial heterogeneity owing to its tree-based algorithm that favours distinct boundaries [4], while MGWR is good at modelling continuous spatial heterogeneity [26,86,87]. Even so, the satisfactory range of model fitness levels varies around and above 50 %, which exhibits strong evidence for the overall contribution of urban morphology parameters to the urban heat [5,8,15,17,30]. Unexplained effects within the models are presumed to stem from natural factors, such as solar radiation levels, humidity, wind profiles, and the green vegetation coverage in the hexagon units as urban proxies.

MGWR and SHAP-explained XGBoost results effectively showed the importance of urban morphological features and their contributions to urban heat heterogeneity ranked from high to low. Even though the XGBoost model did not directly provide regression coefficients similar to MGWR, SHAP values identified correct interactions and revealed feature contributions in global and local contexts. Models were consistent on the dominant impact of GAR and UBP on urban heat with a minimum spatial variability [88,89]. While MGWR revealed a positive dominant relationship within a linear relationship between GAR-LST and UBP-LST, XGBoost was able to extract the non-linear relationship between the pairs. Consistent with the research conducted with linear models widely used in the literature, MGWR signified that an increase in horizontal building density represented by GAR and the number of plots in an urban area created a certain upward trend in urban heat [5,16]. However, the non-linearity extracted by XGBoost showed an upward trend initially, but a diminishing return at a higher value of GAR and UBP. Variations in building density distinctly influence urban heat by manipulating solar radiation exposure, and air circulation [90,91]. Determining the inflection points of this non-linear influence (either increase or decrease) quantitatively is crucial in decision-making processes to create climate-sensitive urban environments.

MGWR, then, highlighted the negatively correlated FAR and XGBoost also confirmed this negative impact of FAR on urban heat. The cooling impact of FAR, which naturally means higher FAR values lower $LSThex_{mean}$, followed a non-linear trend and urban heat did not steadily decrease with the increase in FAR. Both very low and very high FAR values led to reductions in urban heat, with intermediate values contributing more to heat [8,16,34]. Particularly, GAR and FAR are substantial decision components in urban planning; therefore, defining the ranges of marginal effects to positive or negative is vital for planning and design practices to improve the thermal quality of urban life.

The features associated with the architectural morphology of buildings had a relatively low individual contribution to both models; however, results showed that they have the potential to create a cumulative cooling impact on urban heat. Particularly, CON was the dominant feature that both models agreed on its linear impact on urban heat formation. According to the MGWR, the positive correlation between CON and LST meant that an increase in the number of individual building units created a tendency for urban cooling, consistent with the evidence for urban block and plot features. Thus, rather than attached buildings, a molecular layout design with more gaps between buildings reduces sun exposure and radiation absorption by 3D surfaces, facilitates air circulation in the neighbourhood, and balances urban temperatures. This implies that rearrangements of the building architecture, building dimensions, building granularity and layout design, responsively to the background climate, can significantly mitigate urban heat. For instance, orienting the narrow sides of buildings to minimise solar exposure reduces heat absorption and consequently lowers residual heat contributing to increased urban temperatures [92]. However, throughout the reconfiguration of urban layout and building design, the GAR value needs to be constant or decreased; otherwise, an increase in GAR may create a marginal effect to increase the urban heat.

The models also showed that the urban network has relatively limited local influence on urban heat. However, considering the global impact of the urban network parameters in MGWR, city-scale mobility and transport policies can deliver effective results for the mitigation strategies, acting as a complementary feature for multi-scale morphological parameters. Besides, the non-linear relations between urban network parameters, except REA, and LST support the characterisation of threshold values in the urban planning policies and practices to create climate-sensitive environments with reduced urban heat.

Model-specificity facilitates a broader examination of mitigation potentials, moving beyond a 'one-size-fits-all' approach. Certain models demonstrate a superior fit based on the morphological variables and their relationships with the dependent variable utilised in the analysis. In this study, both models have inherent strengths and limitations. MGWR captured spatial heterogeneity, provided localised insights, identified spatial clusters, and assessed the effects of urban features on urban heat. It also required a multicollinearity test to carefully interpretation of local coefficients, and was computationally intensive for large datasets. XGBoost effectively handled non-linear relationships and interactions between features, offered high predictive accuracy, managed large datasets efficiently, and was robust to outliers. Since the complexity of tree-based models and the interpretation difficulties in feature importance, XGBoost required an interpretation method, SHAP, to clarify the results. This study, by comparing an ML model and a spatial statistical model, instils compelling evidence for employing ML in future urban planning research for spatial data analysis and bridges the gap between researchers who favour machine learning and those who prefer conventional spatial statistical models in urban climate assessments. Researchers can adopt a hybrid approach by using MGWR to validate and interpret spatially explicit patterns while relying on XGBoost to explore non-linear relationships and interactions. This dual approach ensures a more comprehensive understanding of the underlying phenomena. Decisions can be guided by integrating the know-how of professionals, prioritising variables with high relevance to the study context, and involving stakeholders to align the outcomes with practical applications.

The research lies on a methodological limitation of surface thermal anisotropy which relates angle-dependent atmospheric path lengths and the limited field of view of sensors on satellite platforms. Surface thermal anisotropy may cause directional variations in retrieved LST depending on the viewing angle and shaded or obscured areas in the three-dimensional urban environment, resulting in an "angular effect" or "anisotropy" of the LST measurements [93–96]. The unavailability of alternative satellite imagery for the same date in Istanbul entailed this unavoidable limitation which should be considered in future methodological settings.

5. Conclusion

This research highlighted the non-stationary relationships based on model-specificity between multi-scale urban morphological features and localised urban heat heterogeneity. Urban morpho-space, including the building, plot, urban block and urban network, undoubtedly stimulated linear or non-linear influences on urban heat at varying weights. Therefore, future urban planning and design agendas, both in developing new urban areas and in urban regeneration processes, need to control the urban thermal environment by regulating the spatial configurations of the urban fabric through morphological components.

Notably, embedding the SHAP method into XGBoost enhanced the interpretability of research outputs, providing a clearer understanding of feature influences on UHI dynamics. In this sense, the research approach increased methodological comprehension and offered operational efficacy, translating results into actual urban contexts. As a relevant solution to uncover the black-box nature of the ML algorithms, this effort has the potential to address the explainable AI in UHI studies.

Correspondingly, results encourage urban planning practitioners to optimise the complex urban ecosystem of multi-scale morphological features by presenting the range of their marginal effects (in terms of warming/cooling) on urban heat. Therefore, the research provides a practical ground to create urban design codes among effective climatic planning strategies for mitigating urban heat and enhancing the thermal quality of urban life. Such design codes necessitate an evaluation of individual urban features and their interactive effects, thereby highlighting the importance of local strategies for optimising urban morpho-space features [8,26].

Two research lines carry the potential to be further explored in the future. As a follow-up study, the quantitative base of the research will be expanded to validate the generalisability of the research findings by including parametric urbanism in the model framework for measuring the impact of generated hypothetical urban settings on UHI. Additionally, future research could incorporate further significant variables, such as envelope reflectivity, surface materials and vegetative coverage, which are crucial components of passive cooling strategies at the urban level. Addressing these factors would offer a more comprehensive understanding of urban heat mitigation strategies. Another discussion can proceed to develop inclusive methodologies to transfer analytical outputs of the research into actionable insights by effectively communicating with stakeholders and urban planners to facilitate relevant strategies for urban heat mitigation. Continued interdisciplinary collaboration will be essential to address given challenges, fostering a deeper understanding of the reciprocal relationships between urban design and climate resilience.

Declaration of generative AI in scientific writing

During the preparation of this work, the author(s) used ChatGPT to improve language and readability. After using this tool/service, the author(s) reviewed and edited the content as needed and take(s) full responsibility for the content of the publication.

CRediT authorship contribution statement

Deniz Erdem Okumus: Writing – original draft, Visualization, Validation, Methodology, Investigation, Formal analysis, Conceptualization. **Mert Akay:** Writing – original draft, Visualization, Validation, Methodology, Investigation, Formal analysis, Conceptualization.

Declaration of competing interest

The authors declare that they have no known competing financial interests or personal relationships that could have appeared to influence the work reported in this paper.

Appendices

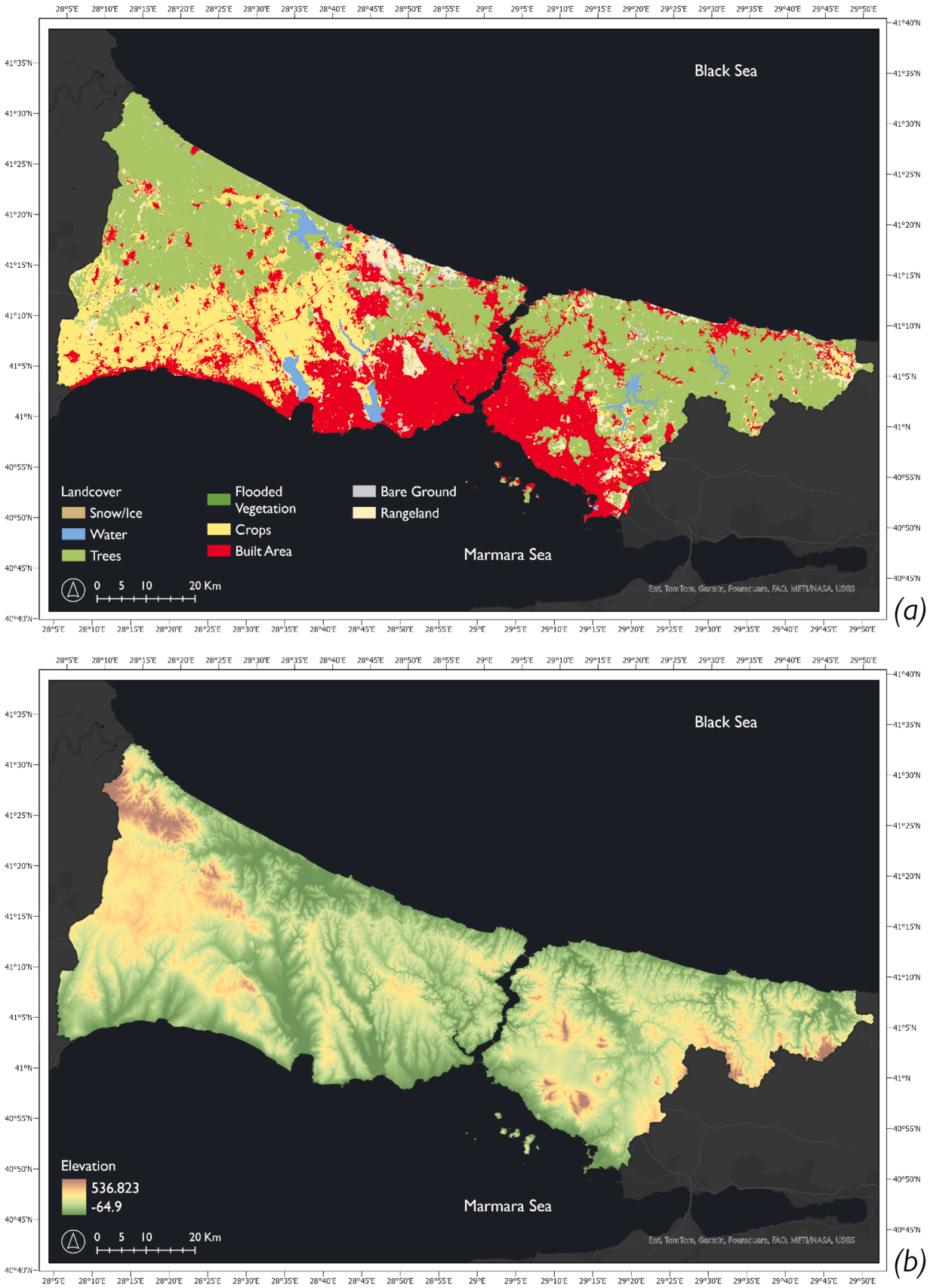

Fig. A.1. Istanbul's land cover map on 2023 (a), and elevation map (b).

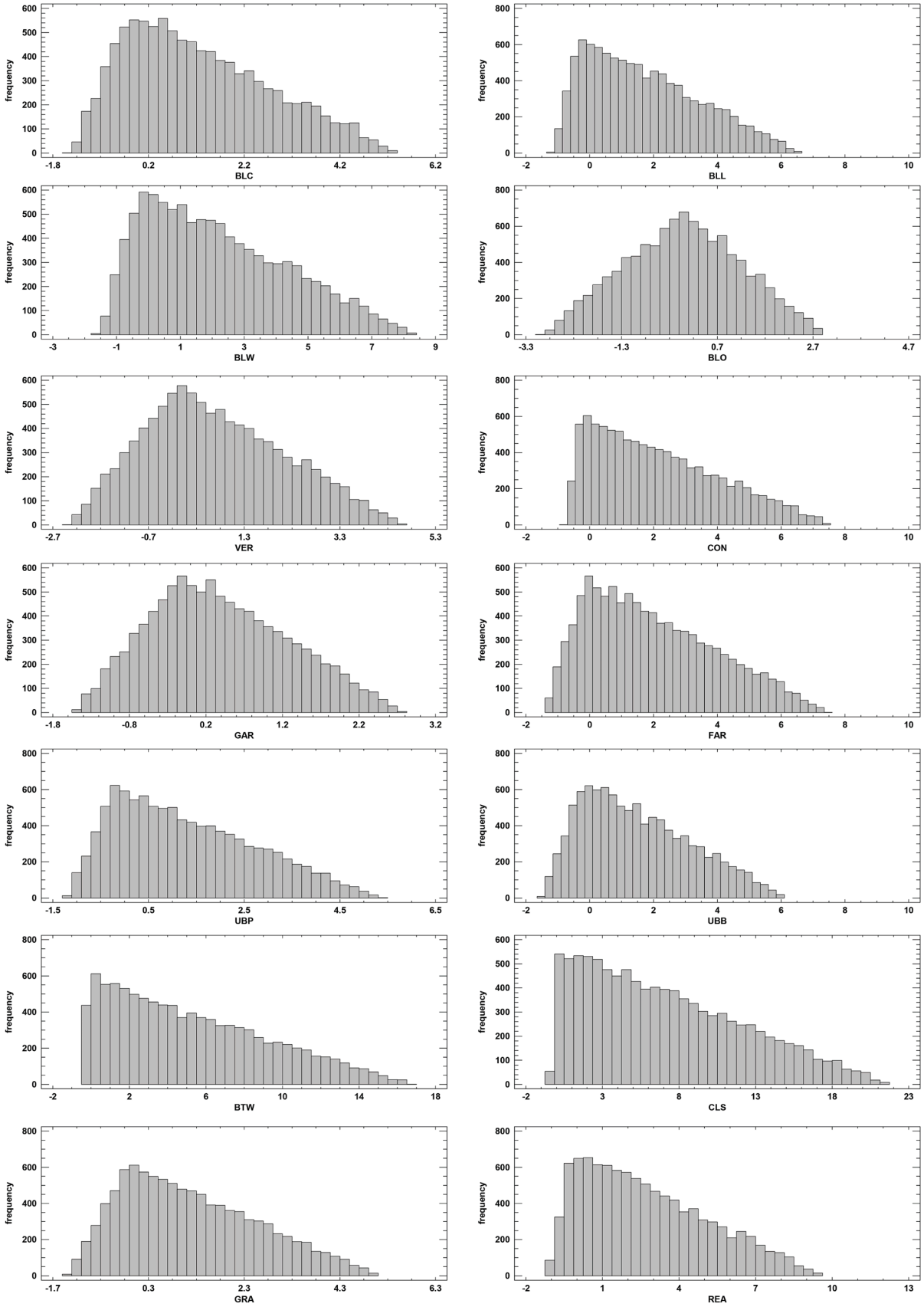

Fig. A.2. Histograms of the simulated dataset.

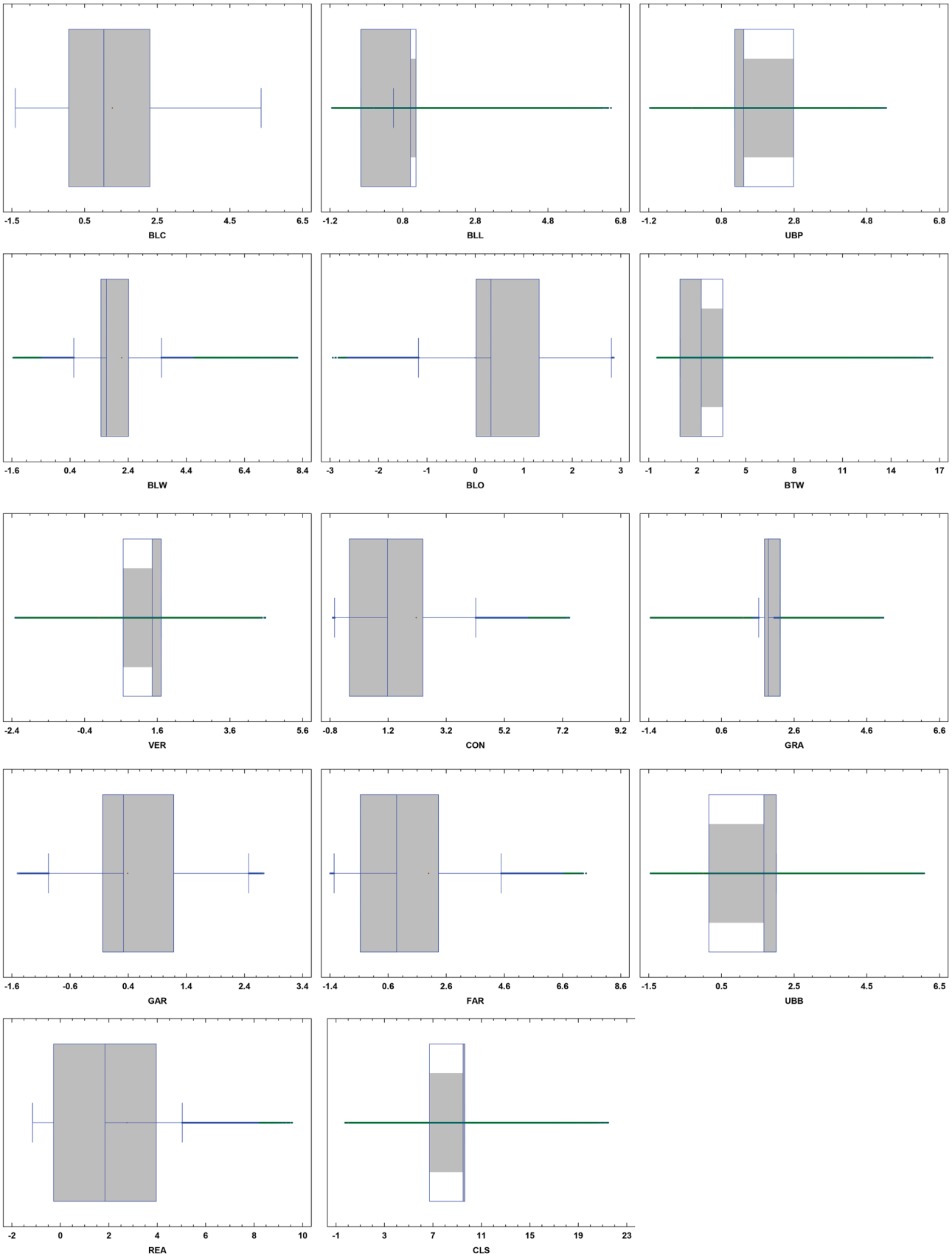

Fig. A.3. The Box and Whisker Plots of the simulated dataset provide insights into data variability and highlight the presence of outliers for each variable.

Table B.1
Descriptive statistics of the simulated test dataset, generated by the combinations of normalised independent variables.

Explanatory Variables	Count	Average	Std.	Minimum	Maximum
$LSThex_{mean}$	10.000	0.203388	0.715894	−2.29163	2.76932
BLC	10.000	1.26194	1.48665	−1.40724	5.35637
BLL	10.000	1.71828	1.742	−1.14481	6.53147
BLW	10.000	2.17552	2.19553	−1.55472	8.21935
BLO	10.000	−0.0071875	1.20289	−2.94206	2.85568
VER	10.000	0.7088	1.45403	−2.30536	4.57465
CON	10.000	2.16745	1.92379	−0.701269	7.43024
GAR	10.000	0.389854	0.895423	−1.50001	2.72579
FAR	10.000	1.98966	1.97008	−1.39003	7.4092
UBP	10.000	1.30689	1.44212	−1.16842	5.3299
UBB	10.000	1.49668	1.67962	−1.45038	6.07726
BTW	10.000	5.25096	4.03934	−0.483057	16.5635
CLS	10.000	7.10822	5.13958	−0.250927	21.47
GRA	10.000	1.19461	1.40733	−1.34944	5.05676
REA	10.000	2.74145	2.42781	−1.14581	9.56453

Std: Standard deviation.

Data availability

Data will be made available on request.

References

[1] J.A. Voogt, T.R. Oke, Thermal remote sensing of urban climates, Remote Sens. Environ. 86 (2003) 370–384.
[2] I.D. Stewart, T.R. Oke, Local climate zones for urban temperature studies, Bull. Am. Meteorol. Soc. 93 (2012) 1879–1900.
[3] S.H. Rizvi, K. Alam, M.J. Iqbal, Spatio-temporal variations in urban heat island and its interaction with heat wave, J. Atmos. Sol. Terr. Phys. 185 (2019) 50–57.
[4] Z. Li, Extracting spatial effects from machine learning model using local interpretation method: an example of SHAP and XGBoost, Comput. Environ. Urban. Syst. 96 (2022) 101845.
[5] D.Erdem Okumus, F. Terzi, Evaluating the role of urban fabric on surface urban heat island: the case of Istanbul, Sustain. Cities. Soc. 73 (2021), https://doi.org/10.1016/j.scs.2021.103128.
[6] IPCC[Core Writing Team H. Lee, K. Calvin, D. Dasgupta, G. Krinner, A. Mukherji, P. Thorne, C. Trisos, J. Romero, P. Aldunce, K. Barret, Climate Change 2023: synthesis Report, summary for policymakers, in: H. Lee, J. Romero (Eds.), Contribution of Working Groups I, II and III to the Sixth Assessment Report of the Intergovernmental Panel On Climate Change, IPC, 2023 [Core Writing Team]2023.
[7] B.S. Sützl, D.A. Strebel, A. Rubin, J. Wen, J. Carmeliet, Urban morphology clustering analysis to identify heat-prone neighbourhoods in cities, Sustain. Cities. Soc. 107 (2024) 105360.
[8] Z. Lin, H. Xu, L. Han, H. Zhang, J. Peng, X. Yao, Day and night: Impact of 2D/3D Urban Features On Land Surface Temperature and Their Spatiotemporal Non-Stationary Relationships in Urban Building Spaces, Sustain Cities Soc, 2024 105507.
[9] H. Hou, H. Su, K. Liu, X. Li, S. Chen, W. Wang, J. Lin, Driving forces of UHI changes in China's major cities from the perspective of land surface energy balance, Sci. Total Environ. 829 (2022) 154710.
[10] T.R. Oke, The urban energy balance, Prog. Phys. Geogr. 12 (1988) 471–508.
[11] Y. Mo, Y. Bao, Z. Wang, W. Wei, X. Chen, Spatial coupling relationship between architectural landscape characteristics and urban heat island in different urban functional zones, Build. Environ. 257 (2024) 111545.
[12] S. Alavipanah, J. Schreyer, D. Haase, T. Lakes, S. Qureshi, The effect of multi-dimensional indicators on urban thermal conditions, J. Clean. Prod. 177 (2018) 115–123.
[13] Z. Liu, L. Hu, H. Chen, Z. Li, L. Jiang, Exploring the combined cooling effect of street canyon geometry and the surrounding built environment, Environ. Sci. Pollut. Res. (2024) 1–18.
[14] Y. Xu, J. Yang, Y. Zheng, W. Li, Impacts of two-dimensional and three-dimensional urban morphology on urban thermal environments in high-density cities: a case study of Hong Kong, Build. Environ. (2024) 111249.
[15] Y. Sun, C. Gao, J. Li, R. Wang, J. Liu, Quantifying the effects of urban form on land surface temperature in subtropical high-density urban areas using machine learning, Remote Sens. (Basel) 11 (2019) 959.
[16] D.Erdem Okumus, F. Terzi, Reconsidering urban densification for microclimatic improvement: planning and design strategies for Istanbul, ICONARP Int. J. Architect. Plan. 10 (2022) 660–687.
[17] X. Ma, J. Yang, R. Zhang, W. Yu, J. Ren, X. Xiao, J. Xia, XGBoost-based analysis of the relationship between urban 2D/3D morphology and seasonal gradient land surface temperature, IEEe J. Sel. Top. Appl. Earth. Obs. Remote Sens. (2024).
[18] Y. Chen, J. Wu, K. Yu, D. Wang, Evaluating the impact of the building density and height on the block surface temperature, Build. Environ. 168 (2020) 106493.
[19] B. Yuan, L. Zhou, F. Hu, C. Wei, Effects of 2D/3D urban morphology on land surface temperature: contribution, response, and interaction, Urban. Clim. 53 (2024) 101791.
[20] S. Guha, H. Govil, A. Dey, N. Gill, Analytical study of land surface temperature with NDVI and NDBI using Landsat 8 OLI and TIRS data in Florence and Naples city, Italy, Eur. J. Remote Sens. 51 (2018) 667–678.
[21] T.M. Logan, B. Zaitchik, S. Guikema, A. Nisbet, Night and day: the influence and relative importance of urban characteristics on remotely sensed land surface temperature, Remote Sens. Environ. 247 (2020) 111861.
[22] Q. Chen, R. Liu, Q. Cheng, Y. Chen, S. Cao, M. Du, K. Li, Evaluating the impact of sky view factor and building shadow ratio on air temperature in different residential and commercial building scenarios: a case study of Beijing, China, Urban. Clim. 49 (2023) 101509.
[23] Y. Ming, Y. Liu, Y. Li, Y. Song, Unraveling nonlinear and spatial non-stationary effects of urban form on surface urban heat islands using explainable spatial machine learning, Comput. Environ. Urban. Syst. 114 (2024) 102200.
[24] J. Chen, W. Zhan, S. Jin, W. Han, P. Du, J. Xia, J. Lai, J. Li, Z. Liu, L. Li, Separate and combined impacts of building and tree on urban thermal environment from two-and three-dimensional perspectives, Build. Environ. 194 (2021) 107650.
[25] Y. Zhang, A. Middel, B.L. Turner, Evaluating the effect of 3D urban form on neighborhood land surface temperature using Google Street View and geographically weighted regression, Landsc. Ecol. 34 (2019) 681–697.
[26] D. Xu, Y. Wang, D. Zhou, Y. Wang, Q. Zhang, Y. Yang, Influences of urban spatial factors on surface urban heat island effect and its spatial heterogeneity: a case study of Xi'an, Build. Environ. 248 (2024) 111072.
[27] Y. Gao, J. Zhao, L. Han, Exploring the spatial heterogeneity of urban heat island effect and its relationship to block morphology with the geographically weighted regression model, Sustain. Cities. Soc. 76 (2022) 103431.
[28] A.S. Fotheringham, W. Yang, W. Kang, Multiscale geographically weighted regression (MGWR), Ann. Am. Assoc. Geogr. 107 (2017) 1247–1265.
[29] R. Lyu, J. Pang, X. Tian, W. Zhao, J. Zhang, How to optimize the 2D/3D urban thermal environment: insights derived from UAV LiDAR/multispectral data and multi-source remote sensing data, Sustain. Cities. Soc. 88 (2023) 104287.
[30] S. Yoo, Investigating important urban characteristics in the formation of urban heat islands: a machine learning approach, J. Big. Data 5 (2018) 2.
[31] C. Fan, S.J. Rey, S.W. Myint, Spatially filtered ridge regression (SFRR): a regression framework to understanding impacts of land cover patterns on urban climate, Transactions GIS 21 (2017) 862–879.
[32] Y. Chen, B. Shan, X. Yu, Study on the spatial heterogeneity of urban heat islands and influencing factors, Build. Environ. 208 (2022) 108604.
[33] Y. Hu, Z. Dai, J.-M. Guldmann, Modeling the impact of 2D/3D urban indicators on the urban heat island over different seasons: a boosted regression tree approach, J. Environ. Manage 266 (2020) 110424.
[34] Z. Lin, H. Xu, X. Yao, C. Yang, D. Ye, How does urban thermal environmental factors impact diurnal cycle of land surface temperature? A multi-dimensional and multi-granularity perspective, Sustain. Cities. Soc. 101 (2024) 105190.
[35] P. Bansal, S.J. Quan, Examining temporally varying nonlinear effects of urban form on urban heat island using explainable machine learning: a case of Seoul, Build. Environ. 247 (2024) 110957.
[36] H. Ahmetoglu, R. Das, A comprehensive review on detection of cyber-attacks: data sets, methods, challenges, and future research directions, Internet Things 20 (2022) 100615, 2022.
[37] J. Zhang, H. Zhang, R. Wang, M. Zhang, Y. Huang, J. Hu, J. Peng, Measuring the critical influence factors for predicting carbon dioxide emissions of expanding megacities by XGBoost, Atmosphere (Basel) 13 (2022) 599.
[38] S.M. Lundberg, S.-I. Lee, A unified approach to interpreting model predictions, Adv. Neural Inf. Process. Syst. 30 (2017).
[39] A.C. Just, K.B. Arfer, J. Rush, M. Dorman, A. Shtein, A. Lyapustin, I. Kloog, Advancing methodologies for applying machine learning and evaluating spatiotemporal models of fine particulate matter (PM2. 5) using satellite data over large regions, Atmos. Environ. 239 (2020) 117649.

[40] D. Chakraborty, H. Başağaoğlu, J. Winterle, Interpretable vs. noninterpretable machine learning models for data-driven hydro-climatological process modeling, Expert. Syst. Appl. 170 (2021) 114498.
[41] H.E. Beck, N.E. Zimmermann, T.R. McVicar, N. Vergopolan, A. Berg, E.F. Wood, Present and future Köppen-Geiger climate classification maps at 1-km resolution, Sci. Data 5 (2018) 1–12.
[42] T.S.M.S., Turkish State Meteorological Service, General Statistical Data of Istanbul, 2018. https://www.mgm.gov.tr/veridegerlendirme/il-ve-ilceler-istatistik.aspx?k=H. accessed March 6, 2020.
[43] F.Bektas Balcik, Determining the impact of urban components on land surface temperature of Istanbul by using remote sensing indices, Environ. Monit. Assess. 186 (2014) 859–872, https://doi.org/10.1007/s10661-013-3427-5.
[44] Y.S. Ünal, C.Y. Sonuç, S. Incecik, H.S. Topcu, D.H. Diren-Üstün, H.P. Temizöz, Investigating urban heat island intensity in Istanbul, Theor. Appl. Climatol. 139 (2020) 175–190.
[45] B. Khorrami, H.B. Heidarlou, B. Feizizadeh, Evaluation of the environmental impacts of urbanization from the viewpoint of increased skin temperatures: a case study from Istanbul, Turkey, Appl. Geomat. 13 (2021) 311–324.
[46] E. Polisciuc, C. Maçãs, F. Assunção, P. Machado, Hexagonal gridded maps and information layers: a novel approach for the exploration and analysis of retail data, in: SIGGRAPH ASIA 2016 Symposium on Visualization, 2016, pp. 1–8.
[47] Y. Duan, C. Yuan, X. Mao, J. Zhao, N. Ma, Influence of the built environment on taxi travel demand based on the optimal spatial analysis unit, PLoS. One 18 (2023) e0292363.
[48] Y.-M.C. Chien, S. Carver, A. Comber, Using geographically weighted models to explore how crowdsourced landscape perceptions relate to landscape physical characteristics, Landsc. Urban. Plan. 203 (2020) 103904.
[49] M. Sajjad, J.C.L. Chan, S.S. Chopra, Rethinking disaster resilience in high-density cities: towards an urban resilience knowledge system, Sustain. Cities. Soc. 69 (2021) 102850.
[50] A.K. Jain, Data clustering: 50 years beyond K-means, Pattern. Recognit. Lett. 31 (2010) 651–666.
[51] K.N.S. Subramaniam, S.R. Bharath, S. Ravinder, Improved authentication mechanism using keystroke analysis, in: 2007 International Conference on Information and Communication Technology, IEEE, 2007, pp. 258–261.
[52] S.K. Singhi, H. Liu, Feature subset selection bias for classification learning, in: Proceedings of the 23rd International Conference on Machine Learning, 2006, pp. 849–856.
[53] M. Karnan, M. Akila, N. Krishnaraj, Biometric personal authentication using keystroke dynamics: a review, Appl. Soft. Comput. 11 (2011) 1565–1573.
[54] USGS, Earthexplorer, (2023). https://earthexplorer.usgs.gov/scene/metadata/full/5e81f14f59432a27/LC81800322023207LGN00/.
[55] USGS, Earthexplorer, (2023). https://earthexplorer.usgs.gov/scene/metadata/full/5e81f14f59432a27/LC81800312023207LGN00/.
[56] J. Barsi, J. Schott, S. Hook, N. Raqueno, B. Markham, R. Radocinski, Landsat-8 thermal infrared sensor (TIRS) vicarious radiometric calibration, Remote Sens. (Basel) 6 (2014) 11607–11626.
[57] USGS, Using the USGS Landsat Level-1 data product, (2013). http://landsat.usgs.gov/Landsat8_Using_Product.php (accessed June 1, 2018).
[58] H. Xu, B. Chen, Remote sensing of the urban heat island and its changes in Xiamen City of SE, J. Environ. Sci. 16 (2004) 276–281.
[59] Q. Weng, D. Lu, J. Schubring, Estimation of land surface temperature–vegetation abundance relationship for urban heat island studies, Remote Sens. Environ. 89 (2004) 467–483.
[60] J.A. Sobrino, J.C. Jiménez-Muñoz, L. Paolini, Land surface temperature retrieval from LANDSAT TM 5, Remote Sens. Environ. 90 (2004) 434–440.
[61] J.C. Jiménez-Muñoz, J. Sobrino, A. Plaza, L. Guanter, J. Moreno, P. Martínez, Comparison between fractional vegetation cover retrievals from vegetation indices and spectral mixture analysis: case study of PROBA/CHRIS data over an agricultural area, Sensors 9 (2009) 768–793.
[62] J.C. Jiménez-Muñoz, J. Sobrino, A. Gillespie, D. Sabol, W. Gustafson, Improved land surface emissivities over agricultural areas using ASTER NDVI, Remote Sens. Environ. 103 (2006) 474–487.
[63] USGS, Landsat 8 Data Users Handbook, 8, Nasa, 2019, p. 97. Version 5.0 November 2019.
[64] WunderUnderground, WunderUnderground, (2023). https://www.wunderground.com.
[65] D.Erdem Okumus, F. Terzi, Ice floes in urban furnace: cooling services of cemeteries in regulating the thermal environment of Istanbul's urban landscape, Urban. Clim. 49 (2023) 101549.
[66] X. Cao, A. Onishi, J. Chen, H. Imura, Quantifying the cool island intensity of urban parks using ASTER and IKONOS data, Landsc. Urban. Plan. 96 (2010) 224–231.
[67] P.M. Schirmer, K.W. Axhausen, A multiscale classification of urban morphology, J. Transp. Land. Use 9 (2016) 101–130.
[68] F. Biljecki, Y.S. Chow, Global building morphology indicators, Comput. Environ. Urban. Syst. 95 (2022) 101809, https://doi.org/10.1016/j.compenvurbsys.2022.101809.
[69] O. Çalışkan, B. Mashhoodi, M. Akay, Morphological indicators of the building fabric: towards a metric typomorphology, J. Urban.: Int. Res. Placemak. Urban Sustain. (2022) 1–30.
[70] M.Y.B. Pont, P. Haupt, Spacematrix: Space, Density and Urban Form-Revised Edition, TU Delft OPEN Publishing, 2023.
[71] A. Sevtsuk, M. Mekonnen, Urban network analysis: a new toolbox for measuring city form in ArcGIS, in: Proceedings of the 2012 Symposium on Simulation for Architecture and Urban Design, 2012, pp. 1–10.
[72] W.G. Hansen, How accessibility shapes land use, J. Am. Inst. Plann. 25 (1959) 73–76.
[73] A. Sevtsuk, R. Kalvo, Modeling pedestrian activity in cities with urban network analysis. Environ Plan B Urban Anal City Sci, 2024 23998083241261770.
[74] R.M. O'brien, A caution regarding rules of thumb for variance inflation factors, Qual. Quant. 41 (2007) 673–690.
[75] A. Wicki, E. Parlow, C. Feigenwinter, Evaluation and modeling of urban heat island intensity in Basel, Switzerland, Climate 6 (2018) 55.
[76] N.M. Zafri, A. Khan, A spatial regression modeling framework for examining relationships between the built environment and pedestrian crash occurrences at macroscopic level: a study in a developing country context, Geogr. Sustain. 3 (2022) 312–324.
[77] T.M. Oshan, Z. Li, W. Kang, L.J. Wolf, A.S. Fotheringham, mgwr: a Python implementation of multiscale geographically weighted regression for investigating process spatial heterogeneity and scale, ISPRS. Int. J. Geoinf. 8 (2019) 269.
[78] B. Liu, X. Guo, J. Jiang, How urban morphology relates to the Urban Heat Island effect: a multi-indicator study, Sustainability. 15 (2023) 10787.
[79] G. Tanoori, A. Soltani, A. Modiri, Machine learning for urban heat island (UHI) analysis: predicting land surface temperature (LST) in urban environments, Urban. Clim. 55 (2024) 101962.
[80] A. Bushenkova, P.M.M. Soares, F. Johannsen, D.C.A. Lima, Towards an improved representation of the urban heat island effect: a multi-scale application of XGBoost for Madrid, Urban. Clim. 55 (2024) 101982.
[81] A. Lin, H. Wu, W. Luo, K. Fan, H. Liu, How does urban heat island differ across urban functional zones? Insights from 2D/3D urban morphology using geospatial big data, Urban. Clim. 53 (2024) 101787.
[82] S.M. Lundberg, G.G. Erion, S.-I. Lee, ArXiv Preprint, 2018.
[83] K.P. Murphy, Machine learning: a Probabilistic Perspective, MIT press, 2012.
[84] P. Harris, A.S. Fotheringham, R. Crespo, M. Charlton, The use of geographically weighted regression for spatial prediction: an evaluation of models using simulated data sets, Math. Geosci. 42 (2010) 657–680.
[85] M. Sachdeva, A.S. Fotheringham, Z. Li, H. Yu, Are we modelling spatially varying processes or non-linear relationships? Geogr. Anal. 54 (2022) 715–738.
[86] L. Niu, Z. Zhang, Z. Peng, Y. Liang, M. Liu, Y. Jiang, J. Wei, R. Tang, Identifying surface urban heat island drivers and their spatial heterogeneity in China's 281 cities: an empirical study based on multiscale geographically weighted regression, Remote Sens. (Basel) 13 (2021) 4428.
[87] S. Çiriş, M. Akay, E. Tümer, Investigating the influence of spatial characteristics on cycling volume: a multi-scale geographic weighted regression approach, Transp. Res. Interdiscipl. Perspect. 26 (2024) 101160.
[88] C. Yin, M. Yuan, Y. Lu, Y. Huang, Y. Liu, Effects of urban form on the urban heat island effect based on spatial regression model, Sci. Total Environ. 634 (2018) 696–704.
[89] G. Guo, X. Zhou, Z. Wu, R. Xiao, Y. Chen, Characterizing the impact of urban morphology heterogeneity on land surface temperature in Guangzhou, China, Environ. Model. Software 84 (2016) 427–439.
[90] W. Liao, T. Hong, Y. Heo, The effect of spatial heterogeneity in urban morphology on surface urban heat islands, Energy Build. 244 (2021) 111027.
[91] J. Yang, B. Shi, G. Xia, Q. Xue, S.-J. Cao, Impacts of urban form on thermal environment near the surface region at pedestrian height: a case study based on high-density built-up areas of Nanjing City in China, Sustainability. 12 (2020) 1737.
[92] H. Farhadi, M. Faizi, H. Sanaieian, Mitigating the urban heat island in a residential area in Tehran: investigating the role of vegetation, materials, and orientation of buildings, Sustain. Cities. Soc. 46 (2019) 101448.
[93] D. Wang, Y. Chen, L. Hu, J.A. Voogt, X. He, Satellite-based daytime urban thermal anisotropy: a comparison of 25 global cities, Remote Sens. Environ. 283 (2022) 113312.
[94] J.-P. Lagouarde, P. Moreau, M. Irvine, J.-M. Bonnefond, J.A. Voogt, F. Solliec, Airborne experimental measurements of the angular variations in surface temperature over urban areas: case study of Marseille (France), Remote Sens. Environ. 93 (2004) 443–462.
[95] J.A. Voogt, T.R. Oke, Complete urban surface temperatures, J. Appl. Meteorol. 36 (1997) 1117–1132.
[96] J.A. Voogt, T.R. Oke, Effects of urban surface geometry on remotely-sensed surface temperature, Int. J. Remote Sens. 19 (1998) 895–920.